NASA TECHNICAL MEMORANDUM

NASA TM X-71955

COPY NO. 1

NASA TM X- 71955

PERFORMANCE OF LI-1542 REUSABLE SURFACE INSULATION SYSTEM IN A HYPERSONIC STREAM

by L. Roane Hunt and Herman L. Bohon

April 1974

This informal documentation medium is used to provide accelerated or special release of technical information to selected users. The contents may not meet NASA formal editing and publication standards, may be revised, or may be incorporated in another publication.

NATIONAL AERONAUTICS AND SPACE ADMINISTRATION

LANGLEY RESEARCH CENTER, HAMPTON, VIRGINIA 23665

1. Report No.	2. Government Accession No.	3. Recipient's Catalog No.
NASA TM X-71955		

4. Title and Subtitle	5. Report Date
PERFORMANCE OF LI-1542 REUSABLE SURFACE INSULATION SYSTEM IN A HYPERSONIC STREAM	April 1974
	6. Performing Organization Code
7. Author(s)	8. Performing Organization Report No.
L. Roane Hunt and Herman L. Bohon	
	10. Work Unit No.
9. Performing Organization Name and Address	
NASA Langley Research Center Hampton, VA 23665	11. Contract or Grant No.
	13. Type of Report and Period Covered
12. Sponsoring Agency Name and Address	High-number TM-X
National Aeronautics and Space Administration Washington, D.C. 20546	14. Sponsoring Agency Code

15. Supplementary Notes

Interim technical information release subject to possible revision and/or later formal publication.

16. Abstract

The thermal and structural performance of a large panel of LI-1542 reusable surface insulation tiles was determined by a series of cyclic heating tests using radiant lamps and aerothermal tests in the Langley 8-foot high-temperature structures tunnel. The test panel was designed by Lockheed Missiles and Space Company to represent a portion of the Space Shuttle Orbiter fuselage along a 1100 K isotherm. Aerothermal tests were conducted at a free-stream Mach number of 6.6, a total temperature of 1830 K, Reynolds numbers of 2.0 and 4.9 X 10^6 per meter, and dynamic pressures of 29 and 65 kPa. The results strongly suggest that pressure gradients in gaps and flow impingement on the header walls at the end of longitudinal gaps are sources for increased gap heating. Temperatures higher than surface radiation equilibrium temperature were measured deep in gaps and at the header walls. Also, the damage tolerance of the LI-1542 tiles appears to be very high. Cracks in the tile coating and craters from foreign particle impact had no apparent effect on tile integrity. Tile edge erosion rate was slow; however, hot gas impingement on the header walls caused excessive erosion, which could not be tolerated in a Shuttle application. Tiles soaked with water and subjected to rapid depressurization and aerodynamic heating showed no visible evidence of damage.

17. Key Words (Suggested by Author(s)) (STAR category underlined)	18. Distribution Statement
Thermodynamics and Combustion Hypersonic Thermal Protection Surface Insulation	Unclassified - unlimited

19. Security Classif. (of this report)	20. Security Classif. (of this page)	21. No. of Pages	22. Price*
Unclassified	Unclassified	55	$3.75

*Available from { The National Technical Information Service, Springfield, Virginia 22151
STIF/NASA Scientific and Technical Information Facility, P.O. Box 33, College Park, MD 20740

PERFORMANCE OF LI-1542 REUSABLE SURFACE INSULATION SYSTEM IN A HYPERSONIC STREAM

by L. Roane Hunt and Herman L. Bohon

Langley Research Center

SUMMARY

The thermal and structural performance of a large panel of LI-1542 reusable surface insulation tiles was determined by a series of cyclic heating tests using radiant lamps and aerothermal tests in the Langley 8-foot high-temperature structures tunnel. The test panel was designed by Lockheed Missiles and Space Company to represent a portion of the Space Shuttle Orbiter fuselage along a 1100 K isotherm. Aerothermal tests were conducted at a free-stream Mach number of 6.6, a total temperature of 1830 K, Reynolds numbers of 2.0 and 4.9 X 10^6 per meter, and dynamic pressures of 29 and 65 kPa. The results strongly suggest that pressure gradients in gaps and flow impingement on the header walls at the end of longitudinal gaps are sources for increased gap heating. Temperatures higher than surface radiation equilibrium temperature were measured deep in gaps and at the header walls. Also, the damage tolerance of the LI-1542 tiles appears to be very high. Cracks in the tile coating and craters from foreign particle impact had no apparent effect on tile integrity. Tile edge erosion rate was slow; however, hot gas impingement on the header walls caused excessive erosion, which could not be tolerated in a Shuttle application. Tiles soaked with water and subjected to rapid depressurization and aerodynamic heating showed no visible evidence of damage.

INTRODUCTION

The thermal protection system (TPS) of the Space Shuttle has been one of the key areas of technological concern since the inception of the Shuttle program (see ref. 1) and will remain so until the system design can be verified through appropriate tests. In support of this need, a test program was initiated to assess the thermal and structural performance of candidate thermal protection systems to identify efficient design features. Several full-scale TPS models, including metallic and reusable surface insulation (RSI), were obtained from industry for thermal-structural cyclic tests in a realistic aerothermal environment. One of the RSI panels is similar to the Shuttle baseline system and test results of this system are reported herein.

The test panel consists of rigidized surface insulation tiles (designated LI-1542) bonded to a substructure. The panel was designed by Lockheed Missiles and Space Company to represent a portion of the Shuttle Orbiter fuselage along a 1100 K isotherm. The model was subjected to several thermal tests including aerodynamic and radiant heating. Aerodynamic heating tests were conducted in the Langley 8-foot high-temperature structures tunnel at a free-stream Mach number of 6.6, a total temperature of 1830 K, Reynolds numbers of 2.0 and 4.9 X 10^6 per meter, and dynamic pressures of 29.0 and 65.0 kPa. The radiant heating tests were performed between aerodynamic heating tests at atmospheric pressure using radiant lamps to simulate the thermal load of the entire Shuttle reentry. Preliminary test results on gap heating, flow impingement, and tile damage tolerance are reported herein.

SYMBOLS

Although physical quantities were measured in U.S. Customary Units, they are presented in this paper in the International System of Units (SI). Factors relating the two systems are given in reference 2 and in the appendix.

p	pressure, Pa
T	temperature, K
t	time, s
x, y, z	model coordinates (see figure 6), m
Δp	differential pressure load on test panel, Pa

APPARATUS AND TESTS

Panel Description

The TPS panel consists of an array of RSI tiles bonded to stringer-stiffened beryllium subpanels mounted on a titanium frame (ref. 3). The model shown in figure 1 is 108 X 152 X 12.7 cm. The primary test article consists of 8 tiles on two subpanels. Top and bottom views of a beryllium subpanel are shown in figure 2. The subpanels are bolted on the titanium frame shown in figure 3. The frame in figure 3(a) is covered by .64 cm titanium plate around the area reserved for the two subpanels. These plates serve as a bonding surface for the peripheral tiles. An aluminum base plate (.8 mm thickness) was attached directly to the bottom of the frame to absorb the internal radiation of the test panel. The

completed metallic structure with an initial layer of silica rubber bond (RTV-560) is shown in figure 4(a). A portion of the panel with the tiles in place but not bonded is shown in figure 4(b).

The RSI tiles (designated LI-1542) are 29.11 X 29.11 X 3.18 cm and consist of rigidized silica fibers (designated LI-1500) with a .25 mm silica carbide coating (designated 0042). A schematic of the tiles and joints is shown in figure 5. The locations of the panel cross-sections are indicated in the plan view in the upper portion of the figure. The details shown are for the border joints around the subpanels, the interior panel gaps, and the common panel joint between the subpanels. (Note the offsets in the tile alignment to interrupt flow in the longitudinal gaps.) The tile edges are undercut (or notched) 1.27 cm to a height of one-half the tile thickness (or 1.59 cm) on all four sides. The surface gaps between tiles are 1.0 mm wide and the tiles are coated on the sides down to the notch. The notch is filled with a thermal seal, a soft silica fibrous material of 96 kg/m^3 density designed to prevent hot gas flow from penetrating the bond and substructure. The top of the thermal seals was coated with the 0042 coating.

Panel Instrumentation

The panel is instrumented with 65 thermocouples; 18 through the tile thickness, 27 in the tile gaps, and 20 at various locations on the substructure. The locations of these thermocouples are indicated by figure 6 and in table I. In figure 6, the plan view of the panel is shown with details of the front and rear subpanels indicated. The specific locations of thermocouples are given in table I by the cartesian coordinates and an alphanumeric system is used to identify longitudinal and lateral rows.

The longitudinal rows are jogged to follow the subpanel offset of 2.5 cm. The individual RSI tiles are identified by Roman numerals and the distribution of the thermocouples in the tiles and tile gaps are indicated by the solid symbols in the plan view. Typical in-depth thermocouples are shown in the tile, the gaps, and on the substructure in sections AA and BB at the bottom of figure 6.

Panel Holder

The panel holder is a rectangular slab with a half-wedge sharp leading edge. Flow trips at the leading edge are used to ensure an even turbulent boundary layer over the entire surface, and side plates are used to eliminate cross-flow. Flow conditions over the surface of the panel holder are described in detail in reference 4. The panel holder with the panel installed is shown in figure 7 at a typical test position, pitched at 15° to the tunnel centerline. The top surface of the test panel is set flush with the surface of the panel holder, and the panel is supported from the bottom with longitudinal structural beams. The pressure in a cavity beneath the test panel is controlled to provide differential pressure loading across the panel.

Facility

The tests were conducted in the Langley 8-foot high-temperature structures tunnel (HTST) which is shown schematically in figure 8. This facility is a hypersonic blowdown wind tunnel which uses the combustion products of methane and air as the test medium and operates at a nominal Mach number of 7, at total pressures between 3.4 and 24.1 MPa, and at nominal total temperatures between 1400 K and 2000 K. Corresponding free-stream unit Reynolds numbers are between 1×10^6 and 10×10^6 per meter.

These conditions simulate the aerothermal flight environment at Mach 7 in the altitude range between 25 and 40 km. More detailed information can be found in reference 4. A radiant heater is available in the facility to preheat the panel prior to insertion into the stream.

Tests and Test Procedures

In the normal mode of wind-tunnel operation, the model is kept out of the stream until hypersonic flow conditions are established. The model is then inserted rapidly into the stream on an elevator and programed through a sequence of events prescribed by test requirements. The model is withdrawn from the stream before tunnel shutdown.

To evaluate TPS concepts, an attempt is made to simulate a generalized temperature history associated with the Shuttle reentry trajectory. The reentry time is too long to be simulated in the relatively short test time of the 8-foot HTST; therefore, the radiant-heat apparatus is used in sequence with the wind tunnel to extend the thermal cycle. The radiant heaters are shown in the cross-section of the test chamber in figure 9. The center sketch shows the tunnel nozzle exit, test chamber, and radiant heaters. The insets show (1) the model in the wind-tunnel test position, (2) the model lowered from the test position and the radiant heaters retracted, and (3) the model covered with the radiant heaters.

Typical surface temperature histories for the three test modes are presented in figure 10. The steps which constitute a particular mode are also defined in the figure. In test mode I, thermal load is provided by radiant heaters. The temperature history of figure 10(a) is representative

of an entire Shuttle reentry thermal cycle. This cycle is characterized by a linear ramp-up of temperature in about 400 s, a temperature hold at about 1100 K for a nominal time of 1500 s, and a controlled cool-down until natural cooling becomes dominate. In test mode II, thermal loading is aerodynamically provided by the tunnel stream. The panel is inserted into the stream at ambient temperature. The surface temperature rises rapidly, approaches a steady-state level within the test duration of about 30 s, and decreases naturally after panel retraction from the stream. Mode III is a combination of mode I and mode II. The nominal hold time is 700 s and the tunnel stream exposure time is 40 s. In this test mode, close coordination is required to remove heaters and then insert the model into the test stream to minimize heat loss between heating periods.

The test panel was exposed to a total of 23 thermal cycles: 11 in mode I, 6 in mode II, and 6 in mode III. The sequence of tests and test conditions are listed in table II. For the radiant heating portions of the tests, the elapsed time during ramp-up and hold at constant surface temperature are tabulated. For the majority of aerodynamic heating tests, the total temperature was nominally 1830 K and the Reynolds number per meter was 4.9×10^6. Nominal test conditions on the panel surface at a 15° pitch angle were a pressure of 15.2 kPa and a dynamic pressure of 171 kPa. Additional tests were also made at zero angle of attack with lower surface static and dynamic pressures. The cavity beneath the panel was, in some tests, vented to the low pressure at the base of the panel holder which developed a collapse pressure (inward acting pressure) over the panel greater than 7 kPa. In other tests, the cavity was sealed from the base

area and the collapse pressure was reduced to .7 kPa. Total test time in the aerodynamic stream is shown for each test.

RESULTS AND DISCUSSION

Thermal Response

All temperature data at a specific reference time are presented in tables III, IV, and V. Temperature data are shown at 1100 seconds into the thermal cycle for radiant heat tests only (table III, mode I) and for aerodynamic heating tests just prior to model insertion (table IV, mode III). The temperature data are grouped for ease of comparison; table III(a) and IV(a) list temperatures through the tile thickness, tables III(b) and IV(b) list temperatures in the tile gaps at 1.59 cm, and tables III(c) and IV(c) list temperatures on the support structure. Table V shows temperature data for all aerodynamic heating tests after 30 seconds in the stream for mode II and 40 seconds in the stream for mode III. It should be noted that most of the temperatures tabulated are transient; however, the surface temperatures are near steady-state.

Typical thermal response at four tile locations is shown in figure 11(a) for a mode II test (test 5) and in figure 11(b) for the aerodynamic phase of a mode III test (test 8). These locations, indicated by the inset, include the tile surface, a longitudinal border gap, and longitudinal and lateral interior gaps.

The thermal response of the border gap and the tile surface is more rapid than that of the interior gaps as indicated in figure 11(a). The maximum temperature of the border gap exceeds that of the surface. The

thermal response of the longitudinal border gap was expected to be similar to that of the longitudinal interior gap; however, this difference is attributed to hot gas leakage through the thermal seal along the border gaps (see figure 5) and will be discussed in detail in a later section.

The temperature history shown in figure 11(b) includes a portion of radiant heating for orientation. The tunnel was started while the lamps were on. During tunnel start, the local static pressure is reduced from atmospheric pressure of 100 kPa to 1.5 kPa in about 5 seconds, and the cool ambient air in the cavity beneath the panel escapes through the thermal seals along the border gaps as reflected by the sharp reduction in border gap temperature. The corresponding interior gap temperatures dropped slightly and the panel surface temperature remain unchanged during this reduction in static pressure. After model insertion, the surface temperature quickly reaches steady-state, or radiation equilibrium, and the border gap temperature (as noted in figure 11(a)) again exceeds the tile surface temperature.

The gap temperatures (solid symbols) and tile temperatures at a depth of 1.27 cm (square symbols) for test 8 are displayed on plan views of the tile array in figure 12. These temperatures are listed in tables IV and V. For comparison, the temperatures recorded at t = 1100 seconds into the radiant heating phase are presented in figure 12(a) and corresponding temperatures recorded at t = 1215 seconds (see time scale of figure 11(b)) are presented in figure 12(b). Generally, the temperatures shown in figure 12(a) are relatively uniform at about 800 K as compared to a surface temperature of approximately 1100 K (table IV). As indicated in figure 12(b), the temperature changed radically during the aerodynamic heating phase.

Temperatures near 1400 K were recorded along the longitudinal border gaps (rows 1 and 5); however, temperatures of the interior gaps (both longitudinal and lateral) were generally around 900 K to 1000 K. The high temperatures at the "header" region - that is, the forward-facing wall at the end of longitudinal gap (for instance, the intersections of rows A3, E3, and I3) - were about 1350 K. The gap temperatures of the header region were expected to be higher than the other gap temperatures because the header region served as a stagnation surface for longitudinal gap flow. The lateral gap temperatures adjacent to the headers in rows A, E, and I are 100 K to 200 K less than the header temperatures, but are generally greater than the interior gap temperatures.

Effects of Differential Pressure

The longitudinal border and subpanel gap temperatures were considerably higher than expected and suggest increased gap flow due to leakage through the thermal seals which permitted hot gas flowthrough to the substructure. The border gap temperature distribution along row 5 is shown in figure 13 for two differential pressure loadings, $\Delta p = 7.6$ kPa (test 8) and $\Delta p = .7$ (test 22). The difference in the temperature levels is indicative of increased gap flow as a result of seal leakage. Reducing the differential pressure resulted in a 100 K to 300 K reduction in border gap temperatures. The substructure temperature at E5 was 500 K during run 8 ($\Delta p = 7.6$ kPa) but only 300 K during test 22 ($\Delta p = .7$ kPa). Consequently, hot gas was apparently leaking to the substructure at E5 where lateral and longitudinal border seals meet. The effects of flow leakage along the longitudinal border gaps on lateral gap temperatures are shown in figure 14 where temperatures along row E are plotted for tests 8 and 22. The header temperature at $y \approx 0$ is

unaffected by Δp. However, the adjacent temperatures, about 15 cm on each side, show 200 K to 300 K reductions when Δp is reduced. Note the difference in the substructure temperatures indicates flowthrough at both corners E1 and E5. These data strongly suggest that gas leakage at the corners causes gap flow transverse to the stream direction. The influence of transverse flow on gap temperature is dependent on the energy of flow in the longitudinal gap approaching the header, which is characterized by the temperature and pressure at the header region.

The interior panel lateral gap temperatures in row G are shown in figure 15 for tests 8 and 22. Here, the effect of pressure gradient is seen to be small due primarily to the absence of an offset (or header) in the longitudinal gap at the center of the subpanel.

After completion of all the tests, the panel was disassembled to examine the regions where hot gas flowed through the thermal seals. The tile array with the forward subpanel removed is shown in figure 16. Much of the fibrous thermal seal was damaged during disassembly. The deep seal in the lateral gap (row E) does not extend to the corner (E5) where high substructure temperatures were noted in figure 14. Evidence of hot gas flow in this region includes an appearance of scrubbing action on the thermal seal and discoloration of the substructure caused by out-gassing of the RTV bond material.

Tile Damage Tolerance

During the test series, the tiles incurred considerable surface damage. In spite of all the surface damage, the array still provided good thermal

performance and appears to have adequate structural integrity. The overall appearance of the tile surface at the conclusion of the tests is shown by the photograph in figure 17. Because of the severity of the test conditions, subsequent tests following the event of surface damage provides some insight into the damage tolerance of the LI-1542 material.

Tile protective coating damage. - The coating is intended to protect the tile from water ingress and to prevent shear erosion of the basic silica tile. Although invisible to the naked eye, cracks were found in the coating before test 4, as indicated in figure 18(a) where the crack pattern is traced on a transparency. During test 4, tunnel flame-out occurred after 6.2 seconds in the stream (see table II); consequently, the hot tiles were exposed to extremely cold flow. A photograph of a typical tile crack pattern after test 4 is shown in figure 18(b). The tile is wetted by a volatile solvent to expose the hairline cracks. All of the tiles were crazed as shown in figure 18(b) after run 4, but did not seem to worsen with repeated tests. There was no flaking of the RSI which suggests the cracks did not penetrate the basic silica tile.

Effects of water soak. - Since the coating crazed and consequently could allow water ingress, tiles VI and VIII were soaked with water for test 23 to determine its effect on tile integrity during rapid change in pressure and temperature. The static pressure and temperature histories for tile VIII are shown in figure 19. The depressurization from 100 kPa to 1.5 kPa occurs during tunnel startup and is followed by a pressure increase as the model is inserted into the stream. For comparison, the Shuttle ascent depressurization rate is shown by the dashed curve. The surface temperature histories

of the soaked tile and an adjacent tile (tile V) with no water are shown on the right of the figure. The temperature of the soaked tile leveled off at the boiling point of water at the local static pressure. However, it is possible that the thermocouple in the soaked tile was shorted by the water; consequently, the surface temperature may have been greater than that shown. Nevertheless, an excessive amount of water was absorbed in the tile and the depressurization rate experienced by the tile was extreme without any evidence of damage to the tile surface.

Foreign particle impact. - During the wind tunnel tests, the model was bombarded with foreign particles inadvertently produced by flaking of the thermal coating of the combustor liner of the 8-foot HTST. Impact of these minute particles caused extensive crater damage to the tiles. A series of photos is shown in figure 20 to illustrate the progression of surface damage. The photos were taken of the same tile after test 8, 12, and 23. The large crater (see large arrow), which appeared after test 8, was field repaired with a mixture of the coating material, and no further erosion was experienced. A smaller crater (see small arrow), which also appeared after run 8, was not repaired and showed no evidence of erosion for the remainder of the tests. Thus, particle impact which caused craters in the RSI tiles had no discernible effect on the tile integrity.

Edge erosion. - The tile assembly had forward-facing steps at two locations; each of which experienced erosion along the tile edges. The progression of edge erosion of a .6 mm step and a .4 mm step is shown in figures 21 and 22, respectively. The propagation of the edge erosion was probably enhanced by foreign particle impact, however, the erosion rate was slow and exposure

of the bare silica to the stream did not result in catastrophic failure. Observation of movie film indicated the eroded edges became local hot spots because of the reduced value of emissivity in the absence of coating.

Flow impingement. - At least one type of damage which cannot be tolerated during a reentry is that due to hot gas impingement in the header region. As noted earlier, temperature at the bottom of the gaps in the header region measured about 1350 K. The resulting damage is shown in figure 23 where the forward-facing wall at the intersection of rows E3 has been eroded about 1 cm into the silica. The temperature in this region must have been near the melting temperature of the silica. This erosion and similar ones at other header regions are significant in the fact that the surface temperature of the tiles was only 1100 K. Consequently, along the bottom centerline of the Orbiter where surface temperatures are around 1600 K, impingement of gap flow on a forward-facing wall could be catastrophic.

CONCLUDING REMARKS

A large panel of LI-1542 RSI tiles was subjected to a series of cyclic heating tests using radiant lamps and aerothermal tests in the 8-foot high-temperature structures tunnel to assess their thermal and structural performance. The results strongly suggest that pressure gradients in gaps and flow impingement on the header walls at the end of longitudinal gaps are sources for increased gap heating. Temperatures higher than the surface radiation equilibrium temperature were measured deep in gaps and at header walls. Also, the damage tolerance of LI-1542 RSI appears to be very high. The silica carbide coating became crazed early in the test program, but had

no apparent effect on tile integrity. Impact of foreign particles in the stream caused craters in the tiles, but field repairs successfully retarded erosion of the impacted area. Tile edge erosion rate was slow and exposure of the bare silica to the stream did not result in catastrophic failure. However, hot gas impingement on the header walls caused excessive erosion, which could not be tolerated in a Shuttle application. Tiles soaked with water and subjected to rapid depressurization and aerodynamic heating sho no visible evidence of damage.

APPENDIX

CONVERSION OF U.S. CUSTOMARY UNITS TO SI UNITS

Factors required for converting U.S. Customary Units to the International System of Units (SI) are given in the following table:

Physical quantity	U.S. Customary Unit	Conversion factor (*)	SI Unit
Density	pcf	16.01846	kilogram/meter^3 (kg/m^3)
Length	in.	0.0254	meter (m)
	ft	0.3048	meter (m)
	per ft	3.28083	per meter (m^{-1})
Pressure	psi	6894.757	pascal (Pa)
Temperature	°R	5/9	kelvin (K)

*Multiply value in U.S. Customary Unit by conversion factor to obtain equivalent value in SI Unit.

Prefixes to indicate multiples of units are as follows:

Prefix	Multiple
kilo (k)	10^3
centi (c)	10^{-2}
milli (m)	10^{-3}

REFERENCES

1. Anderson, Roger A.; Brooks, William A.; Leonard, Robert W.; and Maltz, Joseph: Structures - A Technology Overview. Astronautics and Aeronautics, Vol. 9, No. 2, February 1971, pp. 38-47.

2. Anon.: Metric Practice Guide. E 380-72, Amer. Soc. Testing Mater., June 1972.

3. Burns, A. Bruce: Final Report for Structural Evaluation of Candidate Space Shuttle Thermal Protection Systems. Rep. No. LMSC-D157398 (Contract NAS1-11153) Lockheed Missiles and Space Company, June 26, 1972.

4. Deveikis, William D.; and Hunt, L. Roane: Loading and Heating of Large Flat Plate at Mach 7 in the Langley 8-foot High-Temperature Structures Tunnel. NASA TN D-7275, 1973.

TABLE I.- THERMOCOUPLE LOCATIONS
(a) RSI tile

Thermocouple No.	Tile no.	Row	x, cm	y, cm
z = 0 (surface)				
T8	I	B2	32.4	-10.8
T10	III	B4	32.4	13.3
T21	IV	D4	61.8	15.9
T28	V	F2	90.8	-15.9
T30	VII	F4	90.8	13.3
T39	VI	H2	120.0	-13.3
T41	VIII	H4	120.0	10.8
z = .51 cm				
T5	I	B2	32.4	-13.3
T11	III	B4	32.4	15.9
T36	VI	H2	120.0	-15.9
T42	VIII	H4	120.0	13.3
z = 1.27 cm				
T6	I	B2	32.4	-13.3
T12	III	B4	32.4	15.9
T43	VIII	H4	120.0	13.3
z = 2.29 cm				
T7	I	B2	32.4	-13.3
T13	III	B4	32.4	15.9
T38	VI	H2	120.0	-15.9
T44	VIII	H4	120.0	13.3

TABLE I.- THERMOCOUPLE LOCATION - Continued
(b) RSI tile gap (z = 1.59cm)

Thermocouple No.	Tile no.	Row	x,cm	y, cm
		Border gap, row A		
T1	I	A2	17.8	-13.3
T2	I	A3		1.3
T3	III	A4		15.9
		Subpanel gap, row E		
T23	V	E2	76.2	-15.9
T24	V	E3		- 1.3
T25	VII	E3		1.3
T26	VII	E4		15.9
		Border gap, row I		
T46	VI	I 2	134.6	-15.9
T47	VI	I 3		- 1.3
T48	VIII	I 4		13.3
		Border gap, row 1		
T4	I	B1	32.4	-27.9
T18	II	D1	61.8	-27.9
T27	V	F1	90.8	-30.5
T35	VI	H1	120.0	-30.5
		Border gap, row 5		
T14	III	B5	32.4	30.5
T22	IV	D5	61.8	30.5
T31	VII	F5	90.8	27.9
T45	VIII	H5	120.0	27.9
		Interior gaps		
T9	III	B3	32.4	1.3
T15	II	C7	47.0	-13.3
T16	II	C3		1.3
T17	IV	C4		15.9
T20	IV	D3	61.8	1.3
T32	V	D2	105.4	-15.9
T33	V	D3		- 1.3
T34	VII	D4		13.3
T40	VIII	H3	120.0	- 1.3

TABLE I. - THERMOCOUPLE LOCATIONS - Concluded (c) Substructure		
Thermocouple No.	x, cm	y, cm
Beryllium subpanel skin (z = 3.50 cm)		
T81	32.4	2.5
T82	32.4	0
T85	105.4	6.7
Titanium frame (z = 6.78 cm)		
T59	20.3	0
T61	78.7	-27.9
T63	↓	0
T65	↓	25.4
T67	105.4	-27.9
T69	105.4	25.4
T71	132.1	-27.9
Titanium frame (z = 12.6 cm)		
T60	20.3	0
T62	78.7	-27.9
T64	↓	0
T66	↓	25.4
T68	105.4	-27.9
T70	105.4	25.4
T72	132.1	-27.9
T74	132.1	0
Aluminum base plate (z = 12.7 cm)		
T77	47.0	0
T78	105.4	0

TABLE II. - SEQUENCE OF TESTS AND TEST CONDITIONS OF THE LI-1542 PANEL

Test	Mode*	Radiant Heat		Wind Tunnel		Model					Comments
		Ramp-up time, s	Hold time, s	Total temperature, K	Reynolds No. per meter	Angle of Attack, Degrees	Surface Pressure, kPa	Local Dynamic Pressure, kPa	Collapse Pressure, kPa	Time in stream, s	
1	I	340	350								Tunnel Breakdown
2	II			1830	2.0×10^6	0	.90	29.4	0	2.85	
3	II			1800	2.0	0	.90	29.4	.2	45.8	
4	II			1770	4.9	15	15.2	171.	8.6	6.2	Combustor flameout
5	II			1830	4.9	15	15.2	171.	8.8	29.8	
6	II			1800	4.9	15	15.2	171	8.6	42.6	
7	I	380	780								
8	III	380	790	1830	4.9	15	15.2	171.	7.6	39.8	
9	I	380	1270								
10	III	430	670	1830	4.9	15	15.2	171.	7.2	38.2	
11	III	460	950	1800	4.9	0	2.1	65.3	-.9	40.6	
12	III	440	650	1800	4.9	15	15.2	171.	5.2	39.7	
13	I	530	1410								
14	I	450	630								
15	III	420	650	1830	4.9	15	15.2	171.	8.8	40.0	
16	I	450	1280								
17	I	430	650								
18	I	440	620								
19	I	430	760								
20	I	450	160								
21	I	410	1800								
22	III	430	1070	1830	4.9	15	15.2	171.	.7	40.6	
23	II			1800	4.9	15	15.2	171.	.7	30.6	Water in two tiles

* I - Radiant heating
II - Aerodynamic heating
III - Radiant and aerodynamic heating

TABLE III - MODE I PANEL TEMPERATURES (K) AT t ≈ 1100 s.
(a) RSI tile

Thermo-couple No.	Test No.								
	7	9	13	14	16	17	18	19	20
z = 0 (surface)									
T8	1102	1117	1109	1103	1126	1111	1108	1112	1084
T10	—	—	1054	1049	1069	1057	1053	1058	
T21	1052	1065	1052	1049	1066	1055	1055	1060	1027
T28	1045	1055	1039	1039	1061	1057	1051	1063	1031
T30	—	—	—	—	—	—	—	—	—
T39	1116	1126	1116	1101	1132	1119	1109	1123	1101
T41	1114	1123	1121	1108	1136	1117	1113	1116	1099
z = .51 cm									
T5	1027	1042	1026	1026	1047	1031	1033	1031	1006
T11	965	978	959	962	978	966	968	966	942
T36	1028	1039	1023	1018	1043	1031	1025	1032	1010
T42	1033	1035	1029	1020	1047	1027	1028	1024	1011
z = 1.27 cm									
T6	848	859	831	841	858	844	845	823	822
T12	797	808	776	789	804	792	793	790	769
T43	869	876	854	858	878	862	862	859	844
z = 2.29 cm									
T7	263	608	574	588	599	593	589	586	570
T13	564	571	537	551	561	554	550	547	533
T38	613	559	587	600	611	607	598	601	586
T44	621	628	598	609	622	613	608	606	593

TABLE III.- MODE I PANEL TEMPERATURES (K) AT t ≈ 1100 s -Continued
(b) RSI tile gap (z = 1.59 cm)

Thermocouple No.	Test No.								
	7	9	13	14	16	17	18	19	20
Border gap, row A									
T1	777	808	792	766	807	753	765	757	694
T2	658	736	707	549	674	469	526	492	408
T3	785	818	794	729	794	697	726	729	636
Subpanel gap, row E									
T23	832	844	816	814	838	818	826	826	797
T24	826	860	832	813	850	802	824	816	743
T25	867	891	856	852	877	847	863	859	812
T26	867	894	869	854	894	857	868	864	801
Border gap, row I									
T46	819	833	803	798	827	805	799	803	768
T47	787	811	779	732	789	693	731	731	608
T48	833	847	826	823	844	820	822	819	788
Border gap, row 1									
T4	758	798	768	699	786	669	701	682	536
T18	754	791	753	738	772	713	754	744	688
T27	692	734	696	589	709	584	618	632	509
T35	713	737	715	642	733	674	648	689	620
Border gap, row 5									
T14	740	774	748	695	763	686	692	705	604
T22	795	816	788	788	815	787	767	791	743
T31	694	744	721	659	739	680	669	693	602
T45	742	787	764	703	781	719	703	726	616
Interior gaps									
T9	806	815	787	796	809	794	795	791	760
T15	873	892	861	865	888	865	869	864	829
T16	959	975	947	953	974	957	952	949	916
T17	816	832	806	807	831	809	811	809	774
T20	804	818	787	802	814	805	805	803	777
T32	867	880	846	853	875	862	858	861	837
T33	867	877	856	861	881	866	866	868	843
T34	889	901	876	880	904	887	886	884	865
T40	796	807	777	782	803	789	789	791	768

TABLE III.- MODE I PANEL TEMPERATURES (K) AT t ≈ 1100 s - Concluded
(c) Substructures

Thermocouple No.	Test No.								
	7	9	13	14	16	17	18	19	20
Beryllium subpanel skin (z = 3.50 cm)									
T81	359	364	341	352	354	356	345	342	336
T82	360	366	342	353	356	358	347	343	336
T85	372	377	352	362	367	369	357	356	349
Titanium frame (z = 6.78 cm)									
T59	317	324	308	317	317	322	309	307	302
T61	311	318	302	311	311	317	304	302	297
T63	321	328	311	319	320	325	313	311	306
T65	316	323	306	316	316	321	308	306	301
T67	310	317	301	311	310	316	303	302	297
T69	312	319	303	313	312	318	306	304	299
T71	312	318	313	312	312	317	305	303	295
Titanium frame (z = 12.6 cm)									
T60	296	305	292	303	299	309	294	293	289
T62	296	305	291	301	299	309	293	292	289
T64	296	304	292	302	299	309	294	293	289
T66	296	303	291	302	298	308	293	292	288
T68	296	305	291	301	298	308	294	292	288
T70	296	304	291	301	298	308	294	292	288
T72	296	304	291	300	298	307	293	292	288
T74	295	303	291	300	298	307	293	292	288
Aluminum base plate (z = 12.7 cm)									
T77	298	307	293	304	301	311	296	294	291
T78	298	306	292	302	300	309	295	294	290

TABLE IV. - MODE III PANEL TEMPERATURES (K) AT t ≈ 1100 s
(a) RSI tile

Thermocouple No.	Test No.					
	8	10	11	12	15	22
z = 0 (surface)						
T8	1111	1115	1114	1076	1107	1101
T10	-	1064	1065	1026	1052	-
T21	1101	1070	1058	1023	1052	1042
T28	1092	1057	1057	1018	1050	1032
T30	1109	-	-	-	-	-
T39	1125	1116	1119	1080	1115	1094
T41	1124	1116	1120	1182	1117	1096
z = .51 cm						
T5	1035	1040	1037	997	1029	1031
T11	981	978	975	936	964	961
T36	1037	1032	1032	991	1029	1015
T42	1037	1031	1032	994	1027	1018
z = 1.27 cm						
T6	852	856	850	815	836	844
T12	808	806	801	766	785	788
T43	876	870	868	833	858	855
z = 2.29 cm						
T7	601	602	595	572	584	593
T13	567	564	558	537	546	554
T38	615	612	608	584	598	600
T44	624	621	616	592	606	609

TABLE IV. - MODE III PANEL TEMPERATURES (K) AT t ≈ 1100 s - Continued
(b) RSI tile gap (z = 1.59 cm)

Thermo-couple No.	Test No.					
	8	10	11	12	15	22
Border gap, row A						
T1	819	783	780	744	754	673
T2	820	618	561	543	507	409
T3	841	782	765	724	718	611
Subpanel gap, row E						
T23	873	842	827	797	821	799
T24	899	829	820	782	800	748
T25	916	868	860	824	849	824
T26	926	878	871	828	847	810
Border gap, row I						
T46	830	821	815	772	802	771
T47	831	774	750	713	733	590
T48	846	836	833	798	818	794
Border gap, row 1						
T4	819	752	740	682	669	331
T18	813	771	756	721	736	692
T27	769	681	680	627	612	502
T35	762	703	706	666	681	586
Border gap, row 5						
T14	799	745	733	695	699	596
T22	847	806	799	739	784	756
T31	779	713	708	761	684	608
T45	812	757	750	627	721	620
Interior gaps						
T9	818	812	804	744	794	775
T15	896	884	877	803	863	851
T16	983	973	967	879	957	932
T17	849	827	819	728	804	793
T20	834	813	813	764	802	796
T32	885	872	867	809	858	848
T33	896	876	874	811	865	857
T34	908	896	892	842	884	877
T40	811	801	1120	753	788	779

TABLE IV.- MODE III PANEL TEMPERATURES (K) AT t ≈ 1100 s - Concluded
(c) Substructure

Thermocouple No.	Test No.					
	8	10	11	12	15	22
Beryllium subpanel skin (z = 3.50 cm)						
T81	361	358	353	344	344	357
T82	362	360	327	346	346	358
T85	374	371	366	357	357	402
Titanium frame (z = 6.78 cm)						
T59	323	320	316	310	309	321
T61	317	314	306	304	304	316
T63	327	323	319	314	313	323
T65	323	318	316	308	308	320
T67	317	314	310	303	304	315
T69	318	316	312	306	306	317
T71	317	315	312	306	306	316
Titanium frame (z = 12.6 cm)						
T60	305	303	299	294	294	306
T62	301	303	299	293	294	306
T64	305	303	299	294	294	306
T66	304	303	299	293	294	307
T68	304	303	299	293	294	305
T70	304	302	299	293	294	306
T72	303	302	298	293	293	303
T74	303	301	298	293	294	302
Aluminum frame (z = 12.7 cm)						
T77	307	305	301	296	296	309
T78	306	303	300	295	296	306

TABLE V. - PANEL TEMPERATURES (K) AFTER 30 s OF AERODYNAMIC HEATING FOR MODE II AND 40 s OF AERODYNAMIC HEATING FOR MODE III

(a) RSI tile

Thermocouple no.	Test no.									
	3	5	6	8	10	11	12	15	22	23
z = 0 (surface)										
T8	732	1139	1126	1187	1166	953	1160	1173	1210	1150
T10	684	–	–	–	1157	949	1149	1162	–	1101
T21	766	1239	699	1201	1204	943	1160	1178	1205	1149
T28	694	1093	1081	1176	1152	938	1146	1161	1180	1100
T30	–	1127	1109	1182	–	–	–	–	–	–
T39	699	1113	1102	1186	1163	940	1156	1173	1191	396
T41	667	1089	1074	1183	1162	780	1158	1176	1189	351
z = .51 cm										
T5	370	613	609	1061	1049	950	1037	1052	1080	637
T11	329	479	478	1007	984	922	971	989	1014	503
T36	359	598	594	1056	1039	937	1028	1048	1057	337
T42	352	582	852	1046	1028	938	1020	1039	1052	334
z = 1.27 cm										
T6	293	294	292	858	908	848	819	1093	873	295
T12	294	292	290	821	804	809	769	790	819	292
T43	294	303	319	877	862	856	838	862	879	334
z = 2.29 cm										
T7	293	292	291	620	607	626	577	591	638	290
T13	293	291	290	588	567	591	541	552	598	290
T38	293	291	289	633	616	632	588	606	639	337
T44	293	291	289	639	623	638	597	613	648	333

TABLE V. - PANEL TEMPERATURES (K) AFTER 30 s OF AERODYNAMIC HEATING FOR MODE II AND 40 s OF AERODYNAMIC HEATING FOR MODE III - Continued
(b) RSI tile gap (z = 1.59 cm)

Thermocouple no.	Test no.									
	3	5	6	8	10	11	12	15	22	23
Border gap, row A										
T1	291	507	523	859	804	697	676	833	500	299
T2	293	1138	1112	1274	1247	509	1191	1278	767	497
T3	291	588	594	1042	998	634	954	996	591	406
Subpanel gap, row E										
T23	293	923	920	1146	1095	771	1053	891	904	606
T24	332	1221	1220	1347	1344	794	1313	1323	1351	1200
T25	311	1061	1073	1326	1264	838	1248	1286	1292	1189
T25	296	866	827	1128	1066	712	964	984	773	569
Border gap, row I										
T46	292	1156	1215	1247	1196	726	1098	1081	863	324
T47	299	1158	1181	1340	1332	561	1306	1326	1291	878
T48	292	901	893	1129	1113	767	1058	1078	869	324
Border gap, row 1										
T4	314	1424	1403	1458	1441	471	1417	1451	1394	1371
T18	294	1142	1112	1213	1178	671	1121	1190	969	768
T27	299	1204	1171	1298	1271	542	1253	1282	1236	1127
T35	295	1225	1210	1305	1279	605	1252	1282	1282	854
Border gap, row 5										
T14	294	1199	1196	1326	1338	496	1289	1340	1266	1135
T22	294	1260	1249	1376	1358	706	1330	1377	1273	1122
T31	299	1432	1405	1442	1431	436	1401	1436	1182	1141
T45	281	1204	1198	1282	1259	499	1171	1270	971	651
Interior gaps										
T9	293	903	887	1271	1259	755	1243	1263	1296	1041
T15	292	622	626	1008	979	816	952	972	934	483
T16	301	866	869	1035	1009	891	988	1044	881	571
T17	292	340	339	679	649	709	615	639	619	322
T20	293	713	699	958	926	798	867	919	834	419
T32	293	337	331	876	853	836	822	852	827	320
T33	296	767	717	1018	997	833	983	1009	976	558
T34	294	656	665	1015	980	856	948	998	891	392
T40	292	531	599	936	916	780	894	939	963	351

TABLE V. - PANEL TEMPERATURES (K) AFTER 30 s OF AERODYNAMIC HEATING FOR MODE II AND 40 s OF AERODYNAMIC HEATING FOR MODE III - Concluded
(c) Substructure

Thermo-couple no.	Test no.									
	3	5	6	8	10	11	12	15	22	23
Beryllium subpanel skin (z = 3.50 cm)										
T81	293	295	294	388	372	393	358	360	409	295
T82	293	295	294	391	374	394	360	362	411	295
T85	294	298	296	403	383	406	371	372	419	298
Titanium frame (z = 6.78 cm)										
T59	293	334	324	399	373	339	356	388	351	292
T61	292	391	403	443	416	328	402	442	371	311
T63	293	412	405	365	347	344	336	353	353	304
T65	292	536	519	534	549	337	507	582	353	296
T67	292	304	302	350	337	327	327	332	347	305
T69	292	331	331	393	387	332	367	387	357	299
T71	292	322	316	363	357	328	343	359	339	305
Titanium frame (z = 12.6 cm)										
T60	292	292	293	311	306	305	296	297	313	291
T62	292	292	293	310	306	304	294	297	314	291
T64	292	292	293	313	307	306	297	298	316	291
T66	292	293	292	310	306	304	297	299	314	291
T68	292	293	293	309	304	305	295	297	312	291
T70	292	291	290	309	304	304	296	297	313	292
T72	291	292	291	311	307	302	296	299	309	292
T74	292	292	291	309	303	302	296	297	309	291
Aluminum base plate (z = 12.7 cm)										
T77	292	293	295	318	314	309	302	308	322	290
T78	292	293	293	318	311	308	303	306	317	292

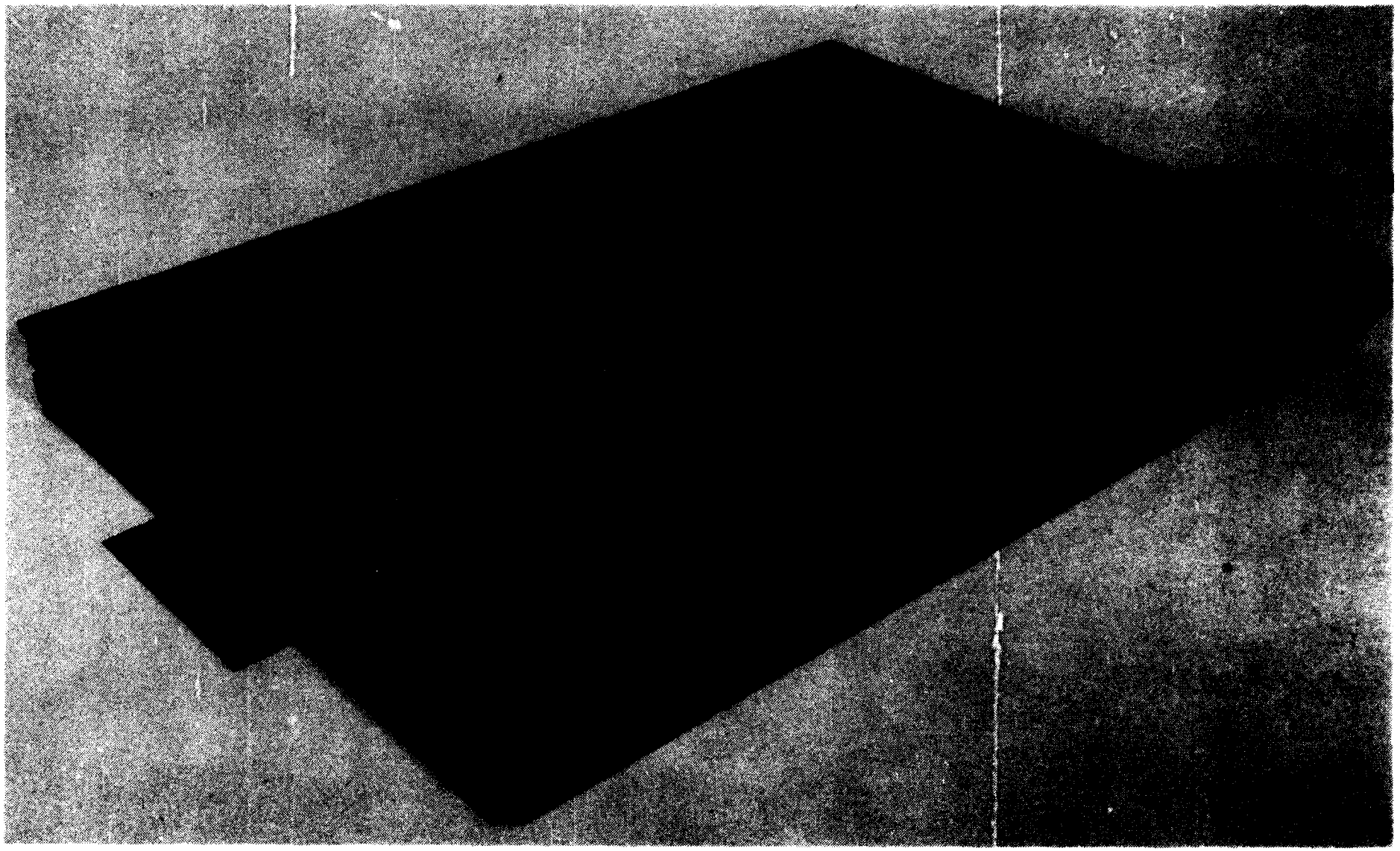

Figure 1. - Photograph of test panel with RSI tiles.

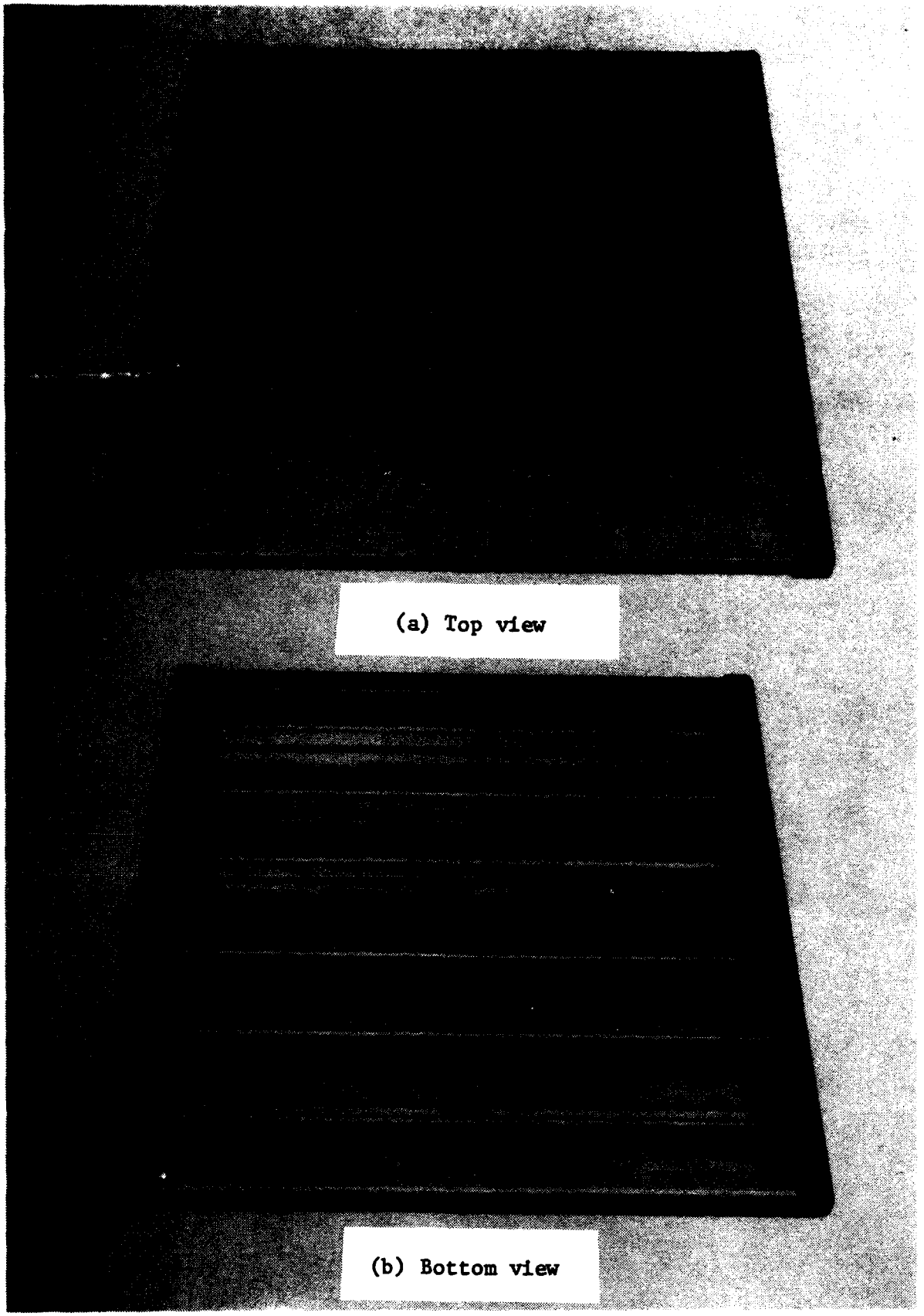

Figure 2. - Photographs of stringer-stiffened beryllium subpanel.

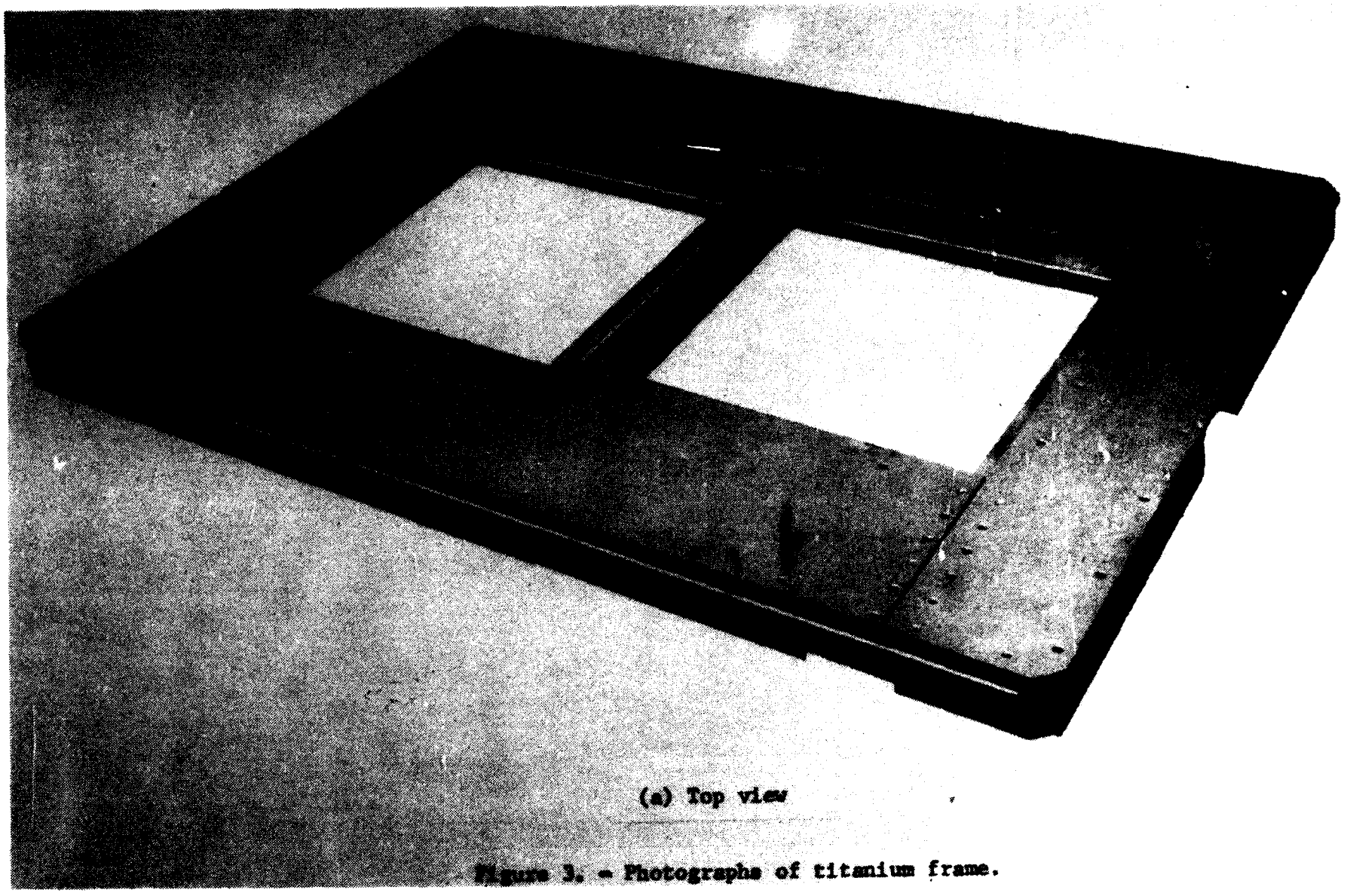

(a) Top view

Figure 3. - Photographs of titanium frame.

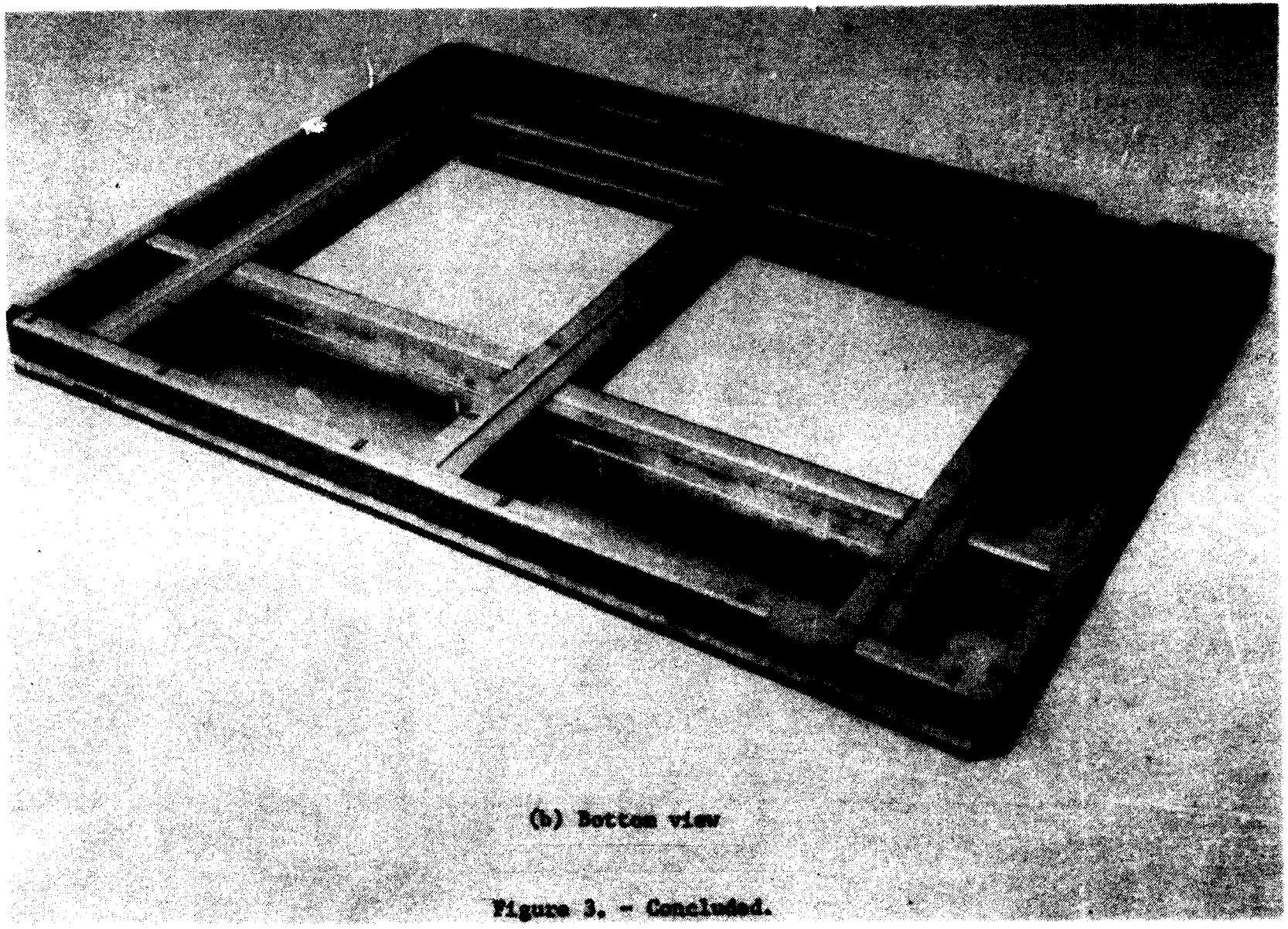

(b) Bottom view

Figure 3. - Concluded.

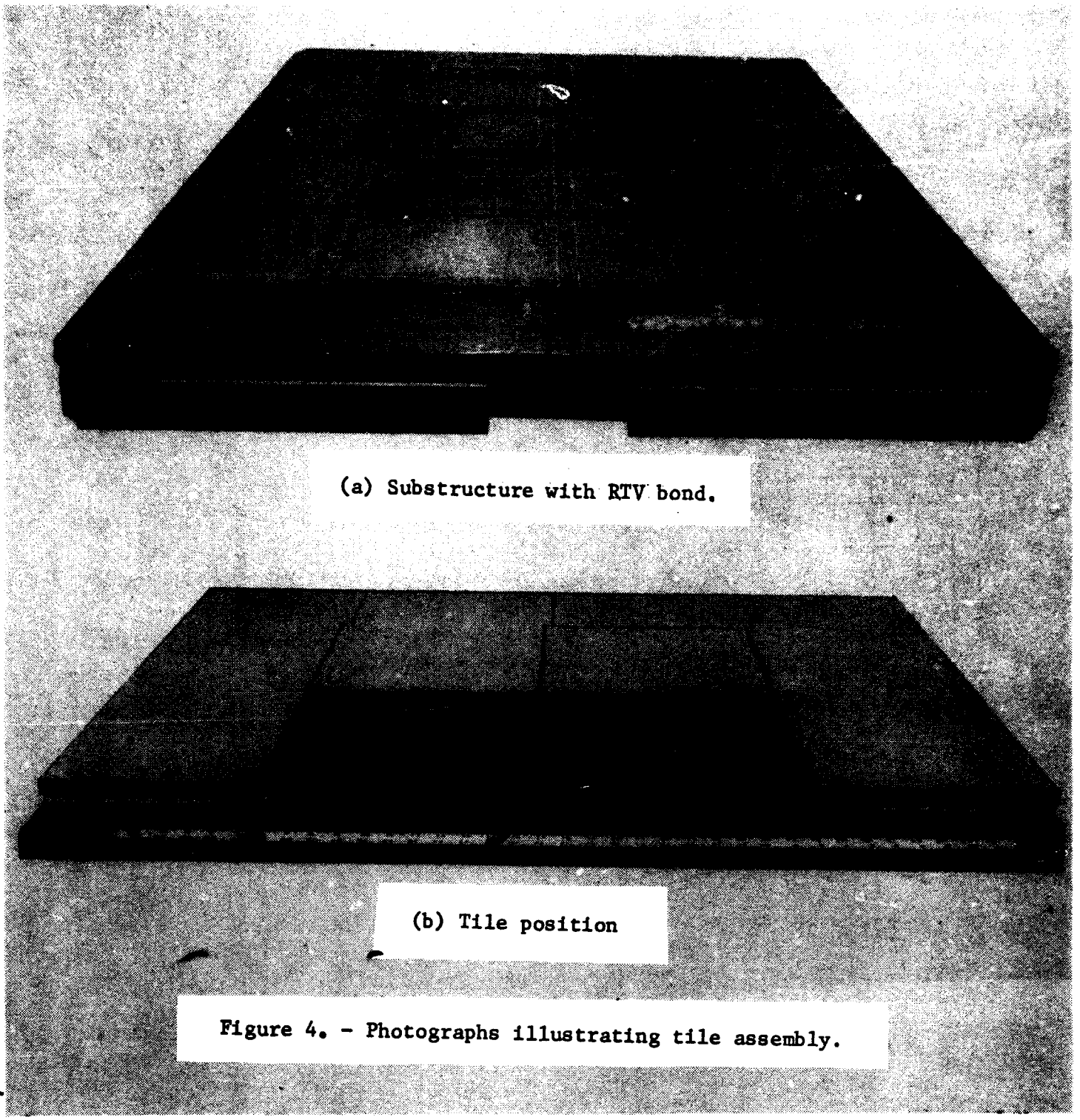

(a) Substructure with RTV bond.

(b) Tile position

Figure 4. - Photographs illustrating tile assembly.

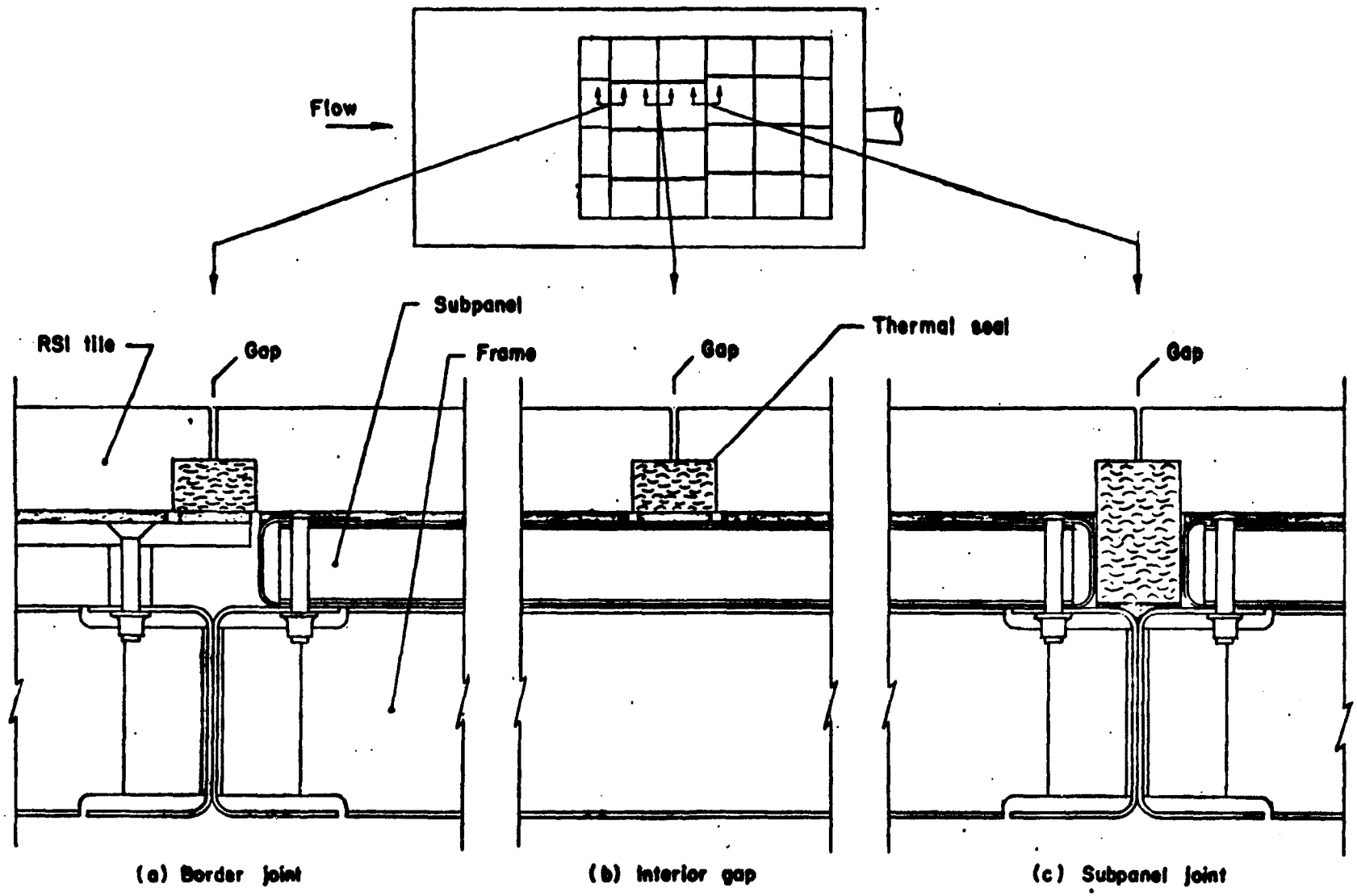

Figure 5.— Skematic of panel tiles and joints.

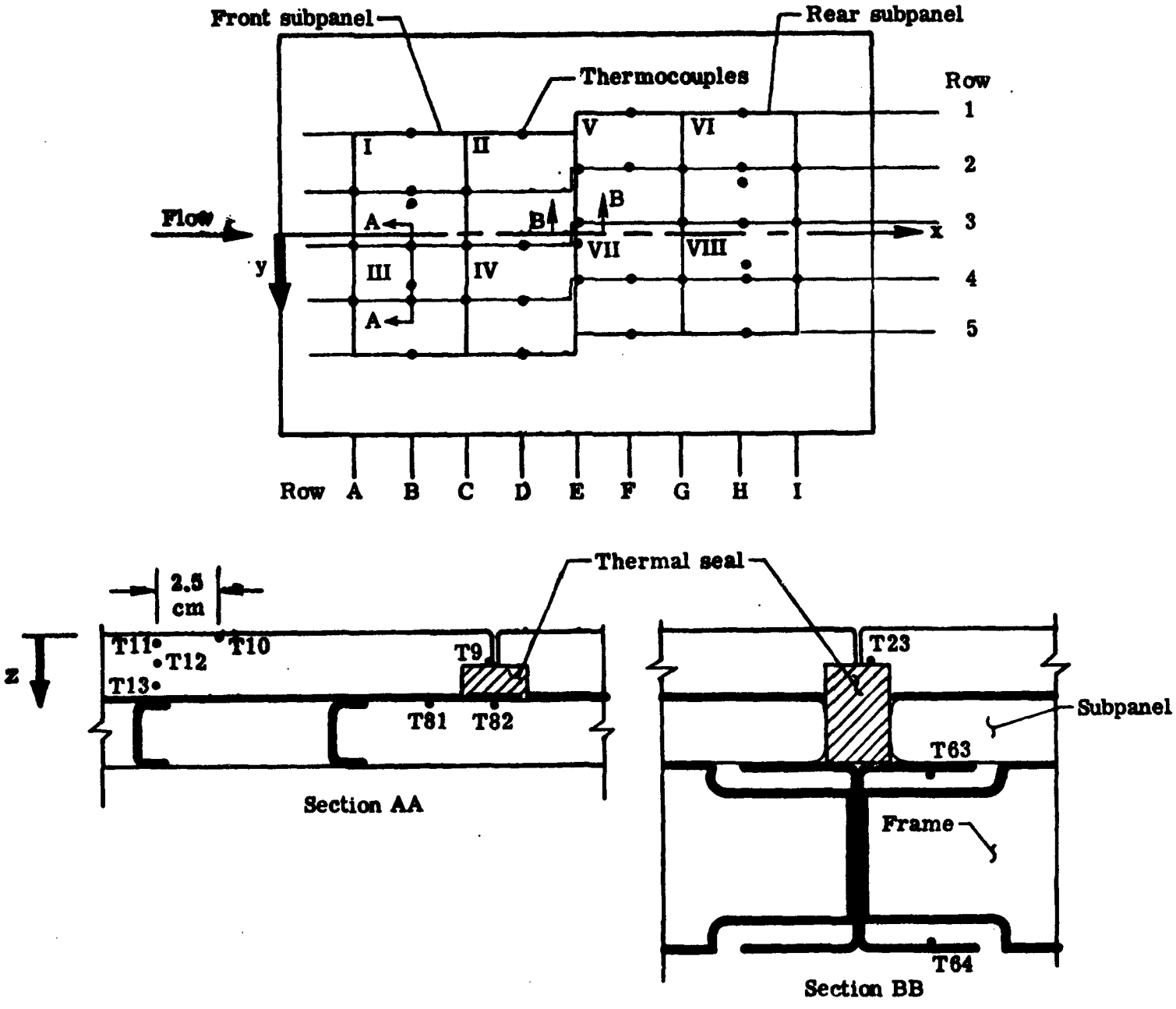

Figure 6.- Sketch of panel structure with thermocouple locations indicated.

Figure 7. - Photograph of test panel installed in the 8-foot HTST panel holder.

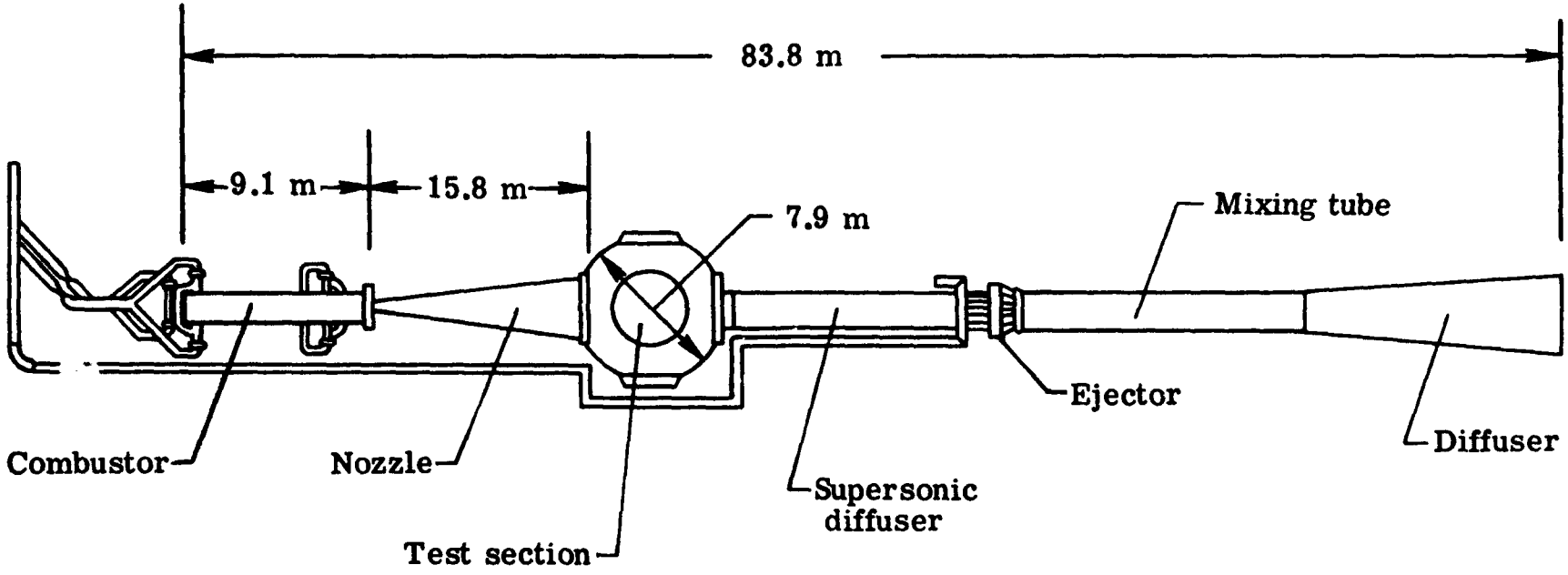

Figure 8.- Schematic drawing of the Langley 8-foot high-temperature structures tunnel.

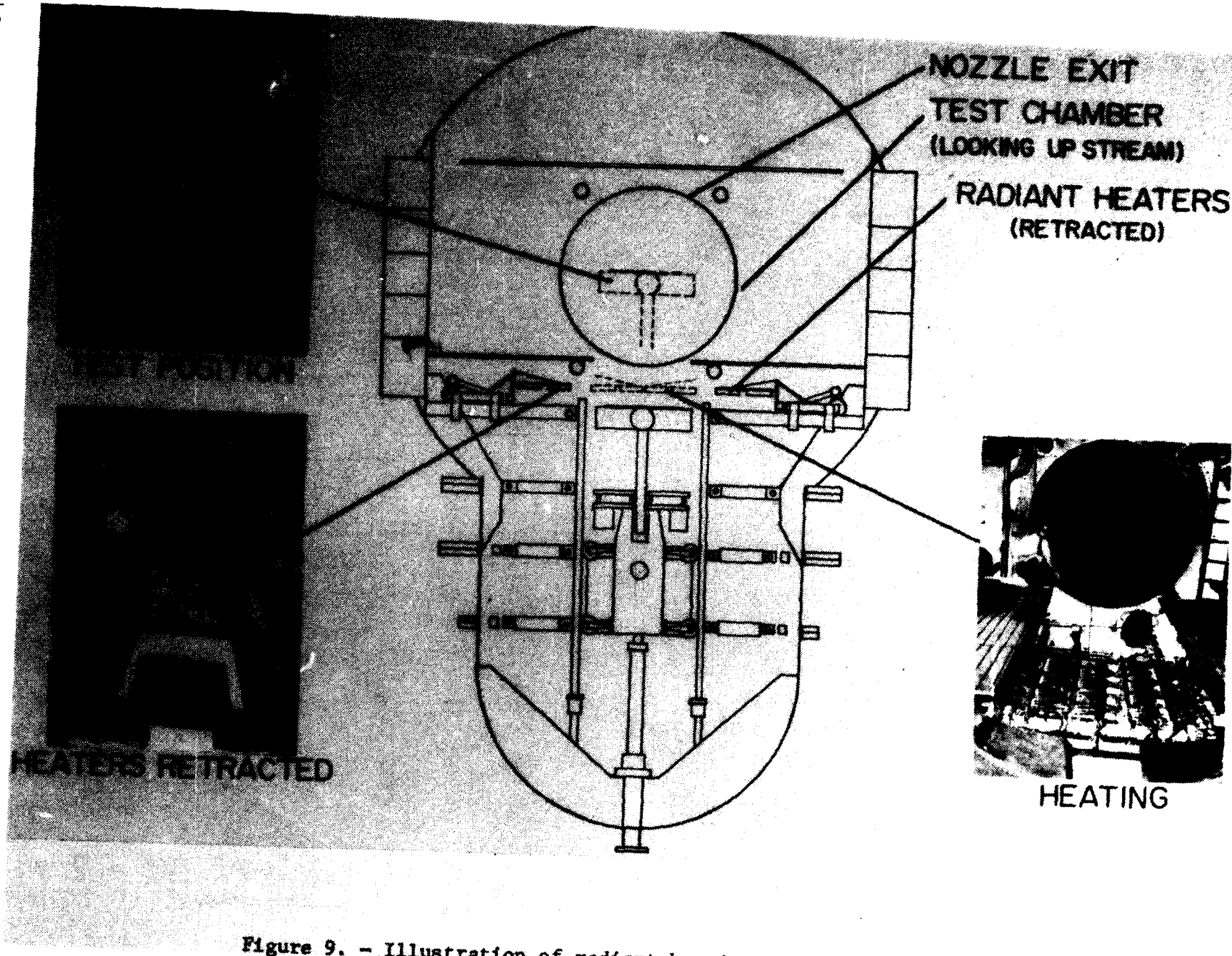

Figure 9. - Illustration of radiant heating apparatus in the 8-foot HTST.

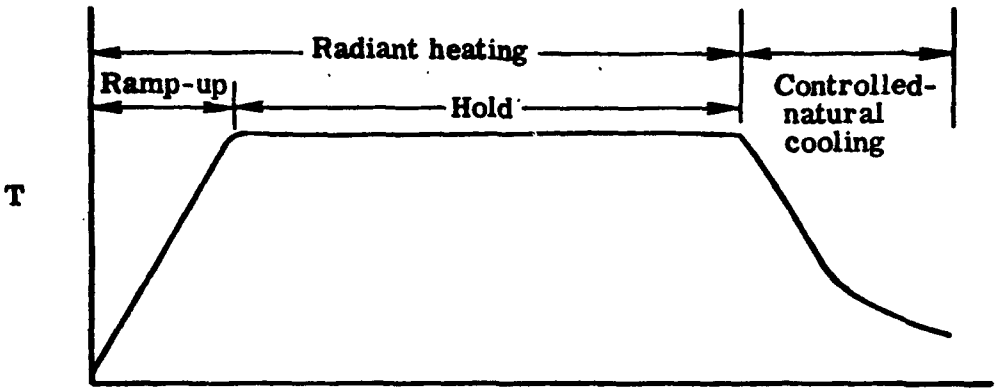

(a) Radiant heating (Mode I).

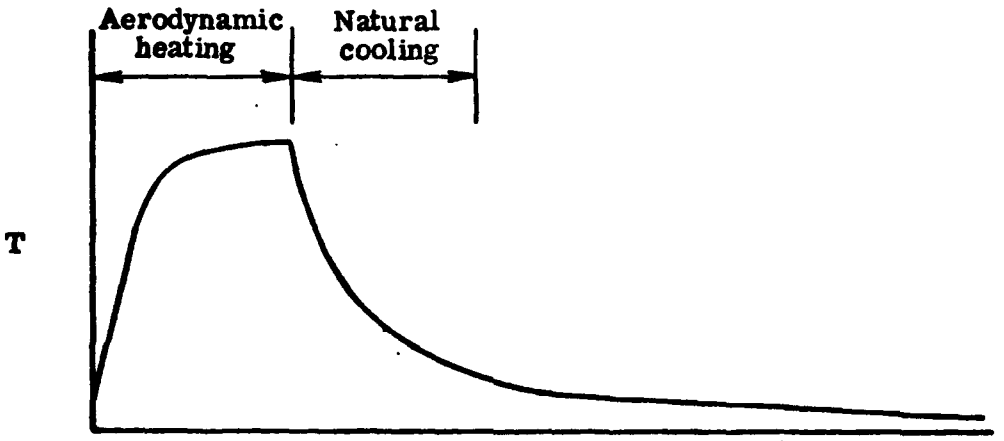

(b) Aerodynamic heating (Mode II).

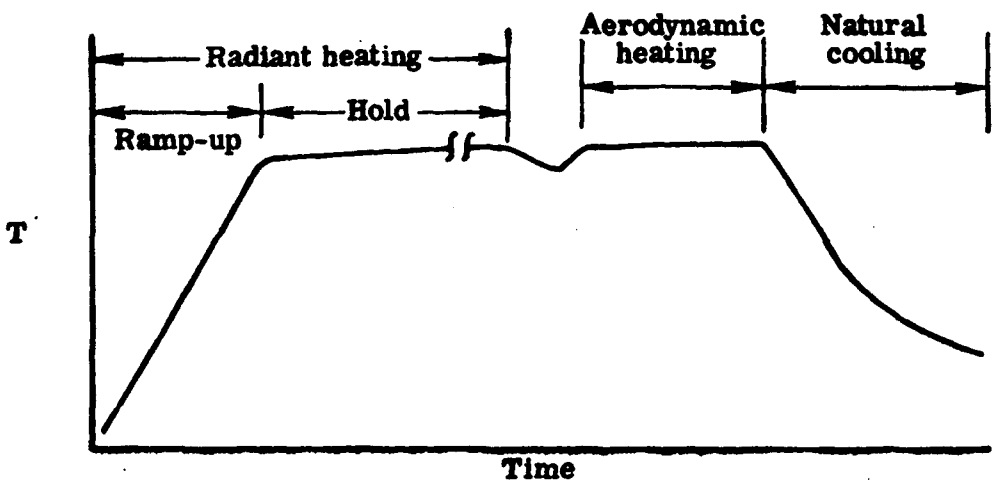

(c) Radiant heating and aerodynamic heating (Mode III).

Figure 10.- Typical surface temperature history test modes.

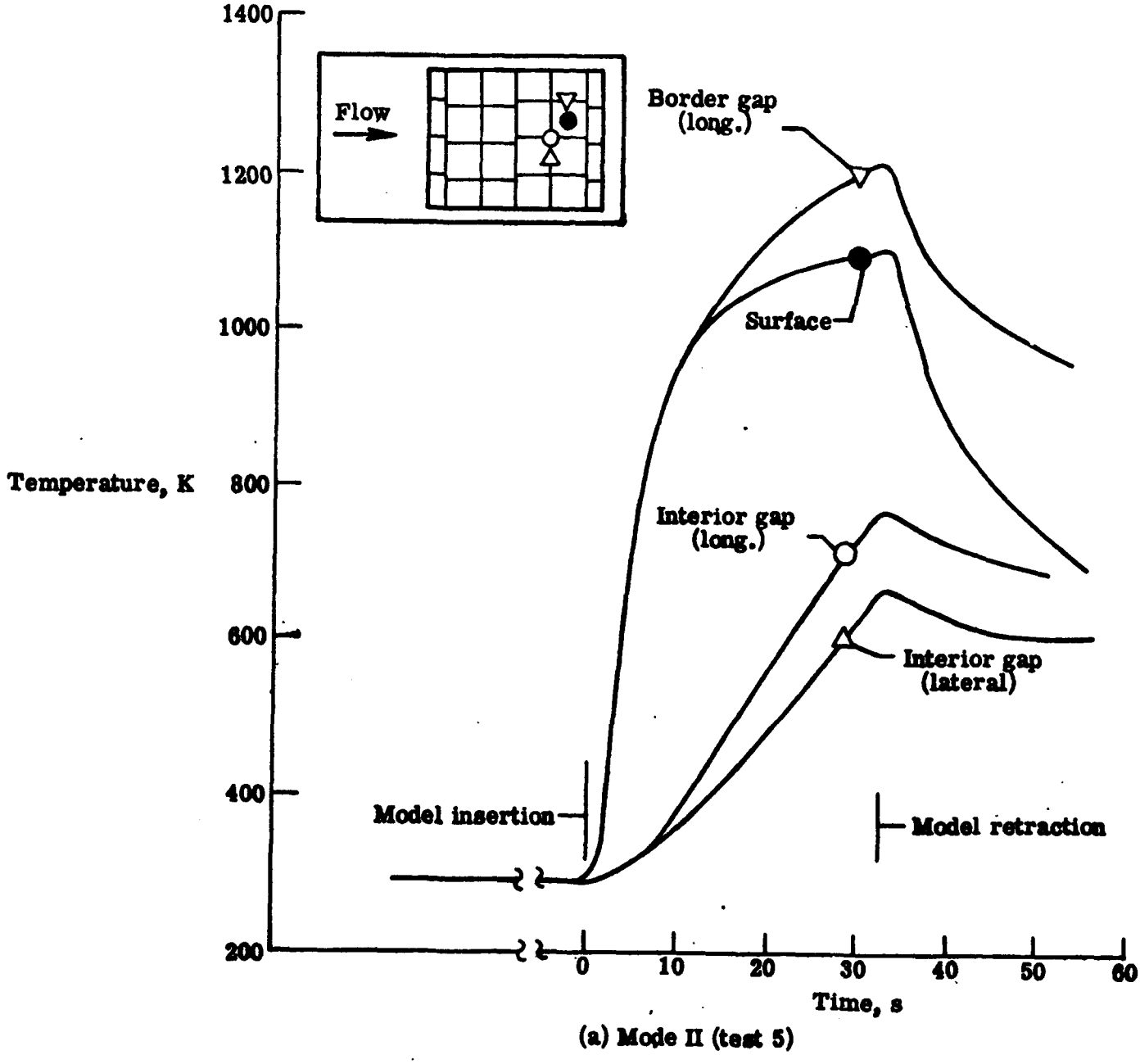

(a) Mode II (test 5)

Figure 11.- Typical thermal response of panel to aerodynamic heating.

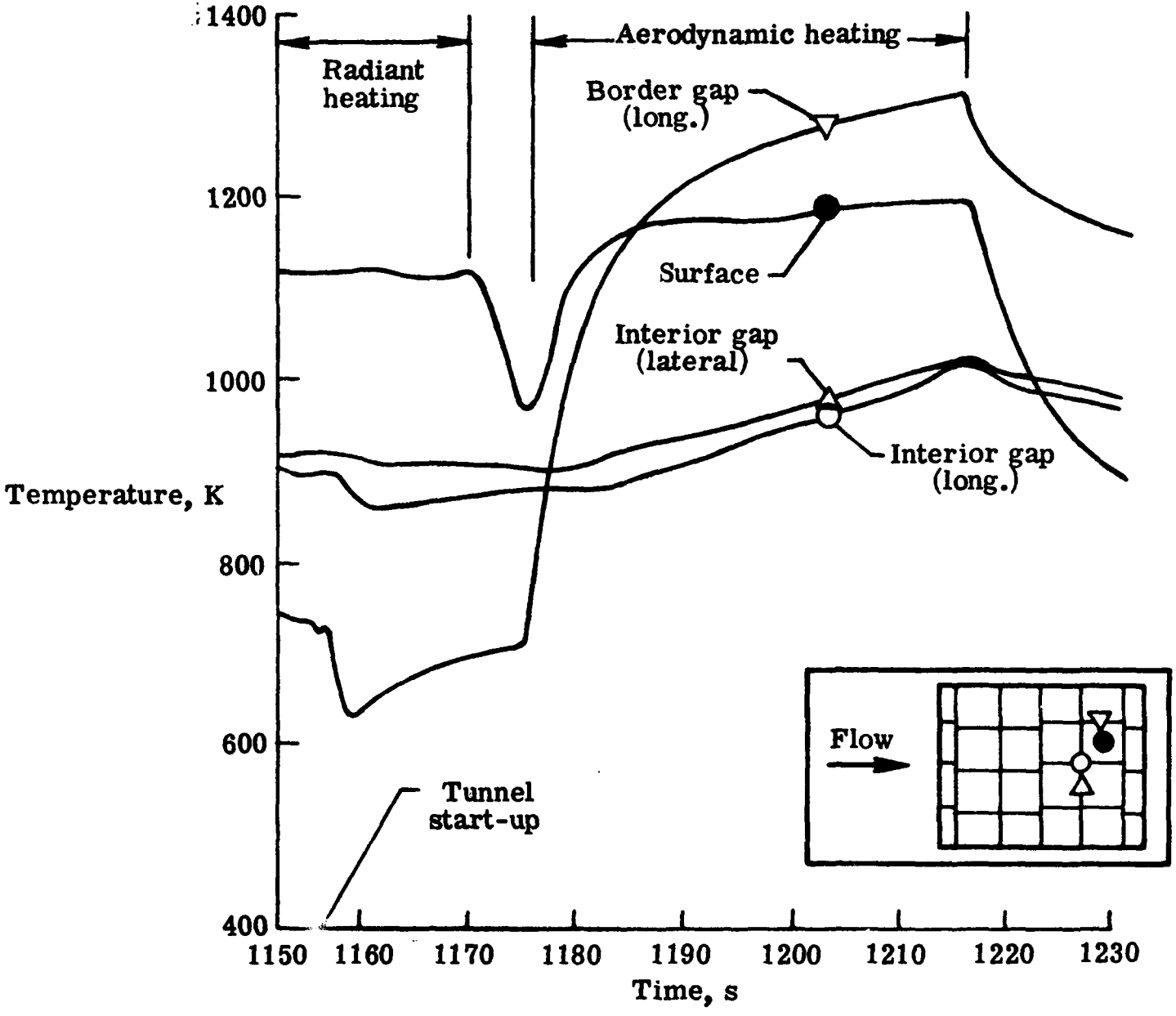

(b) Mode III (test 8)

Figure 11.- Concluded.

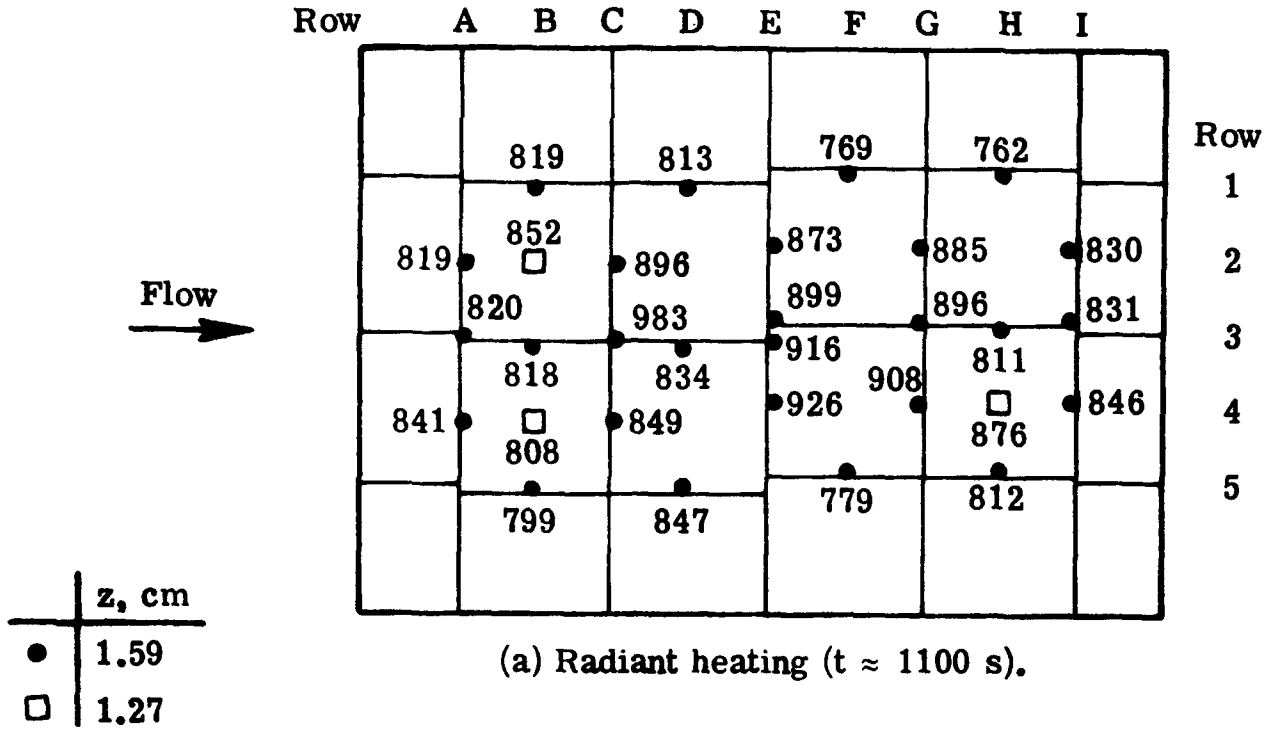

(a) Radiant heating (t ≈ 1100 s).

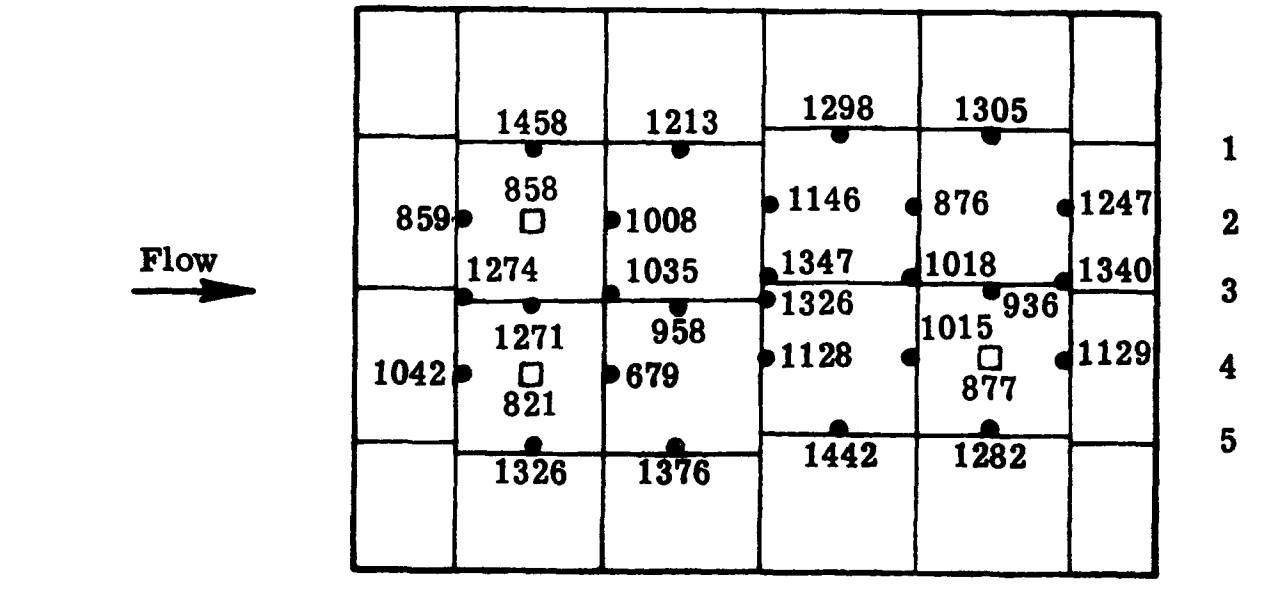

(b) Aerodynamic heating (t = 1215 s)

Figure 12.- Typical temperatures (K) for mode III test (test 8).

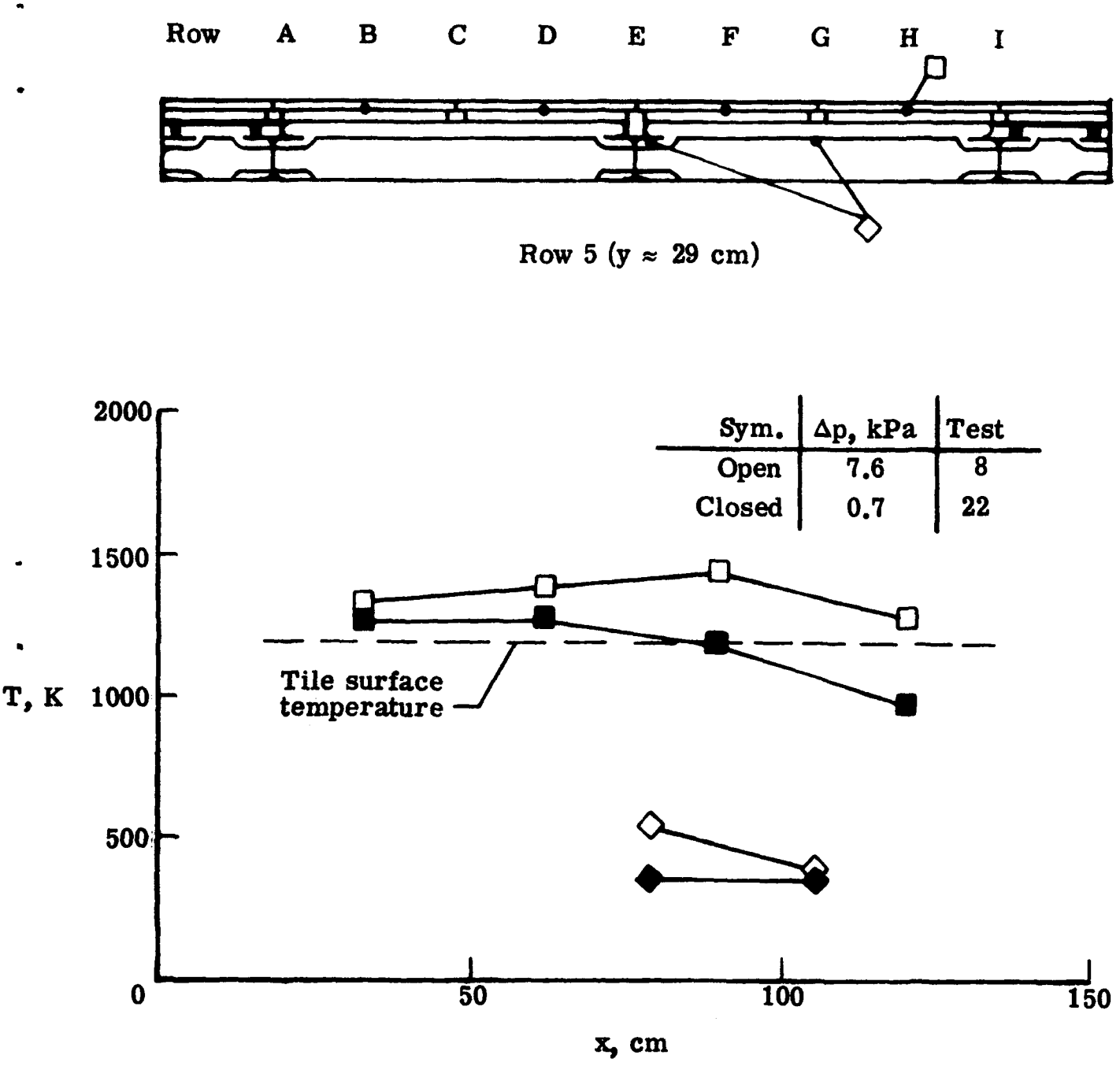

Figure 13.- Effects of differential pressure on gap and substructure temperature along row 5 after 40 s of aerodynamic heating.

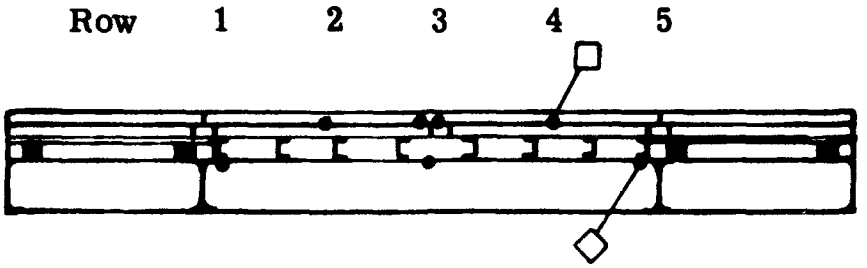

Row E (x = 76.2 cm)

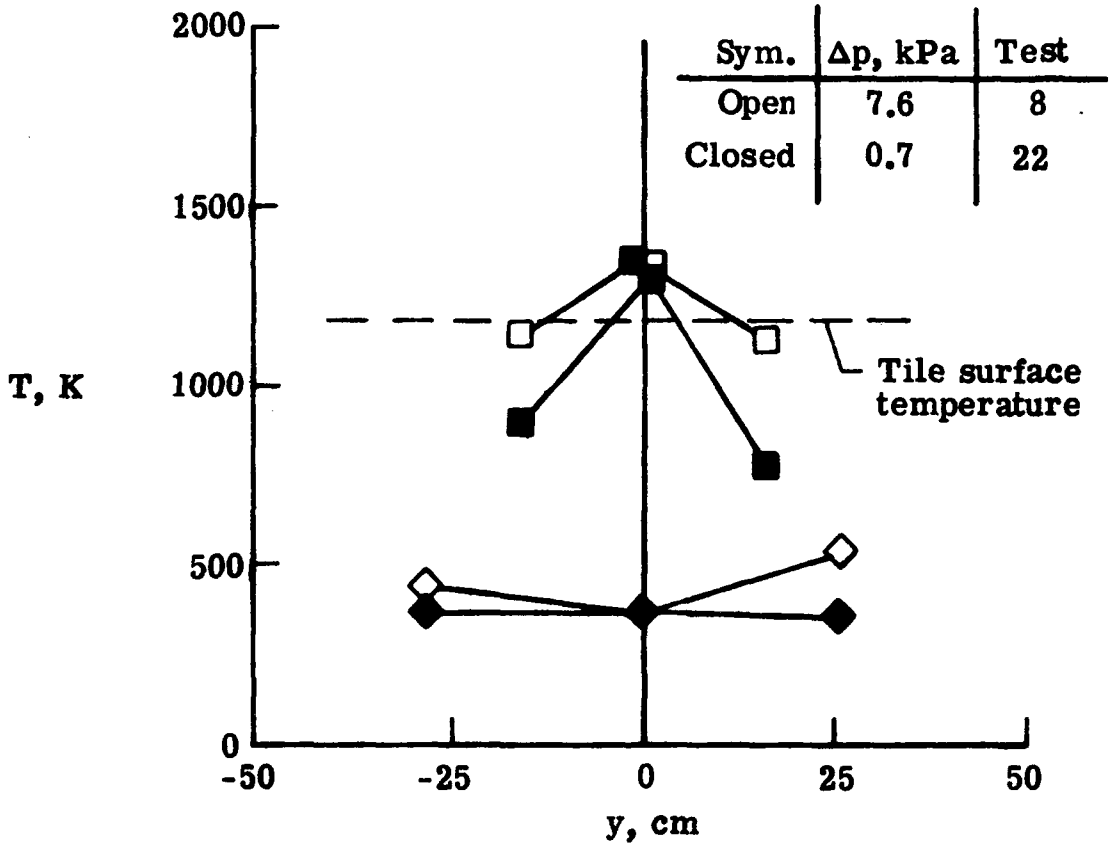

Figure 14.- Effects of differential pressure on subpanel gap and substructure temperature along row E after 40 s of aerodynamic heating.

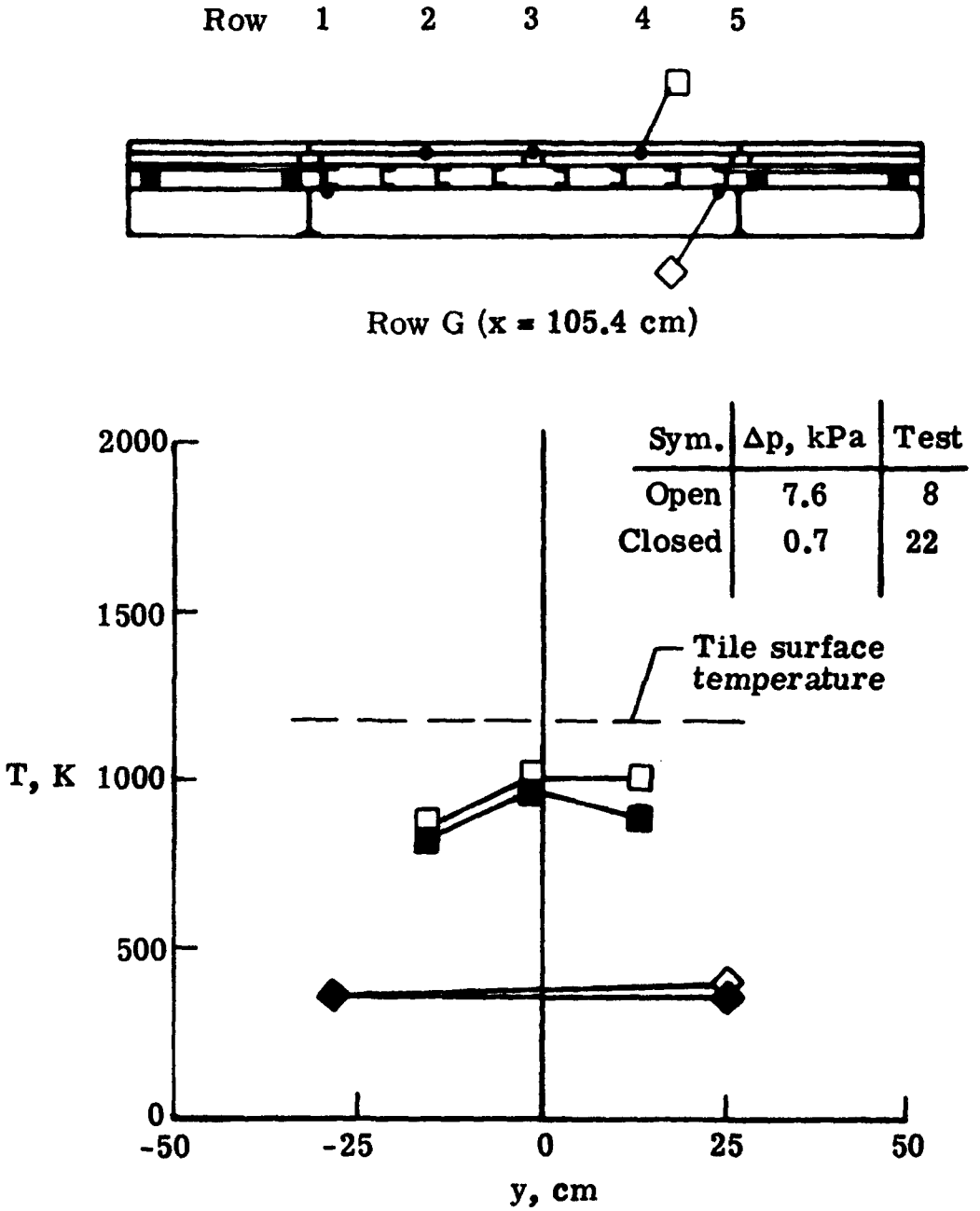

Figure 15.- Effects of differential pressure on interior gap and substructure temperature along row G after 40 s of aerodynamic heating.

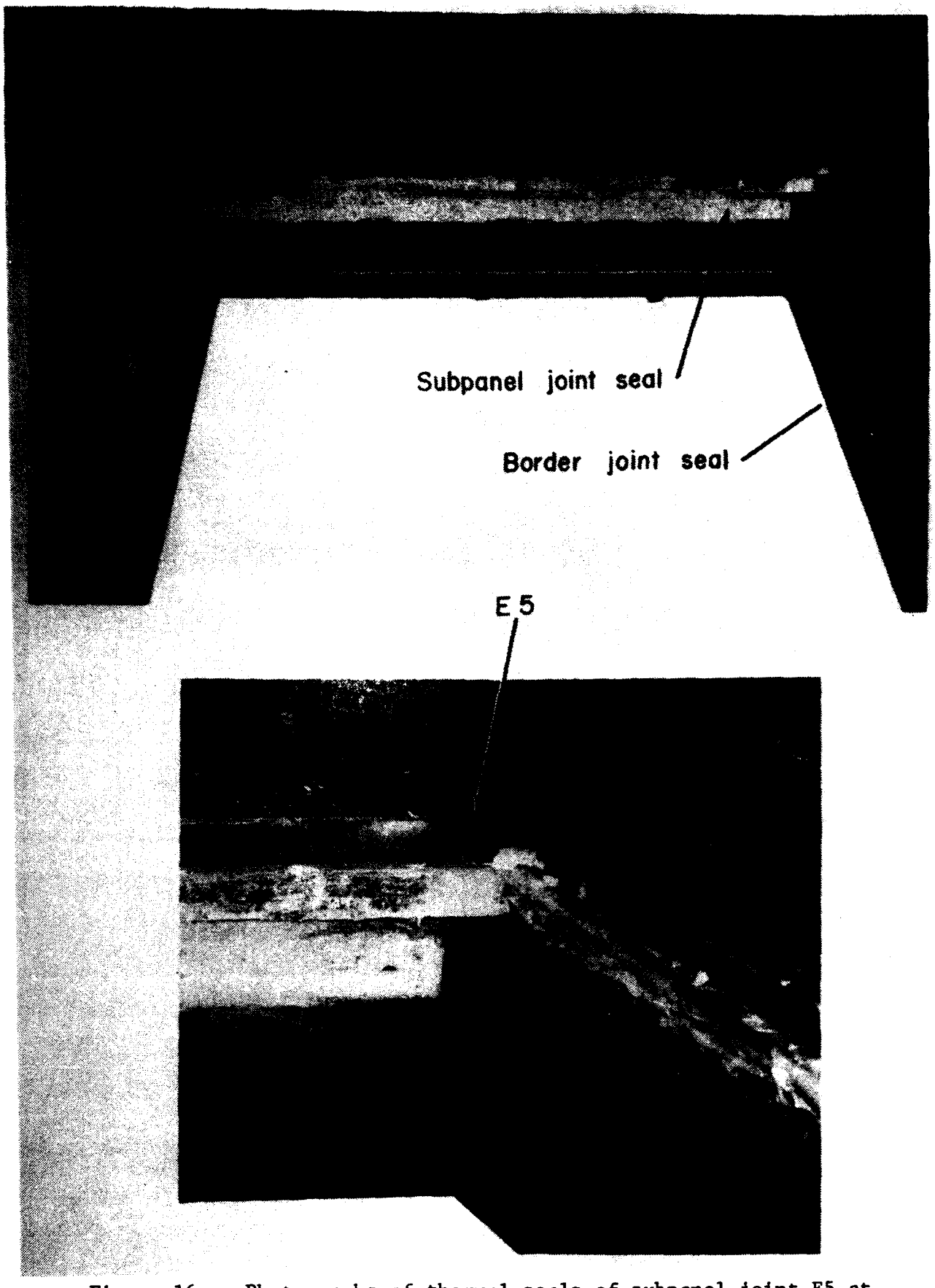

Figure 16. - Photographs of thermal seals of subpanel joint E5 at conclusion of tests.

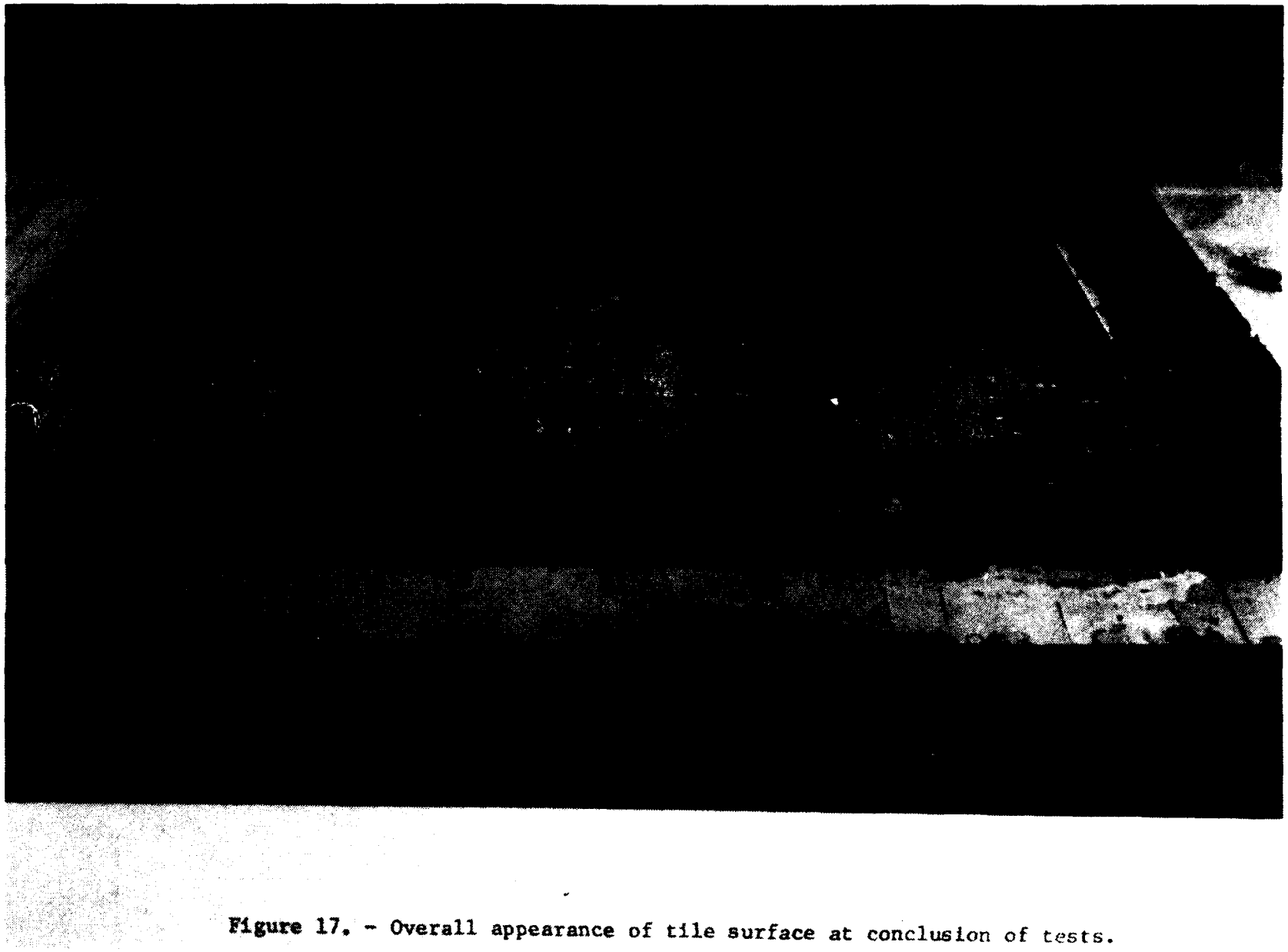

Figure 17. - Overall appearance of tile surface at conclusion of tests.

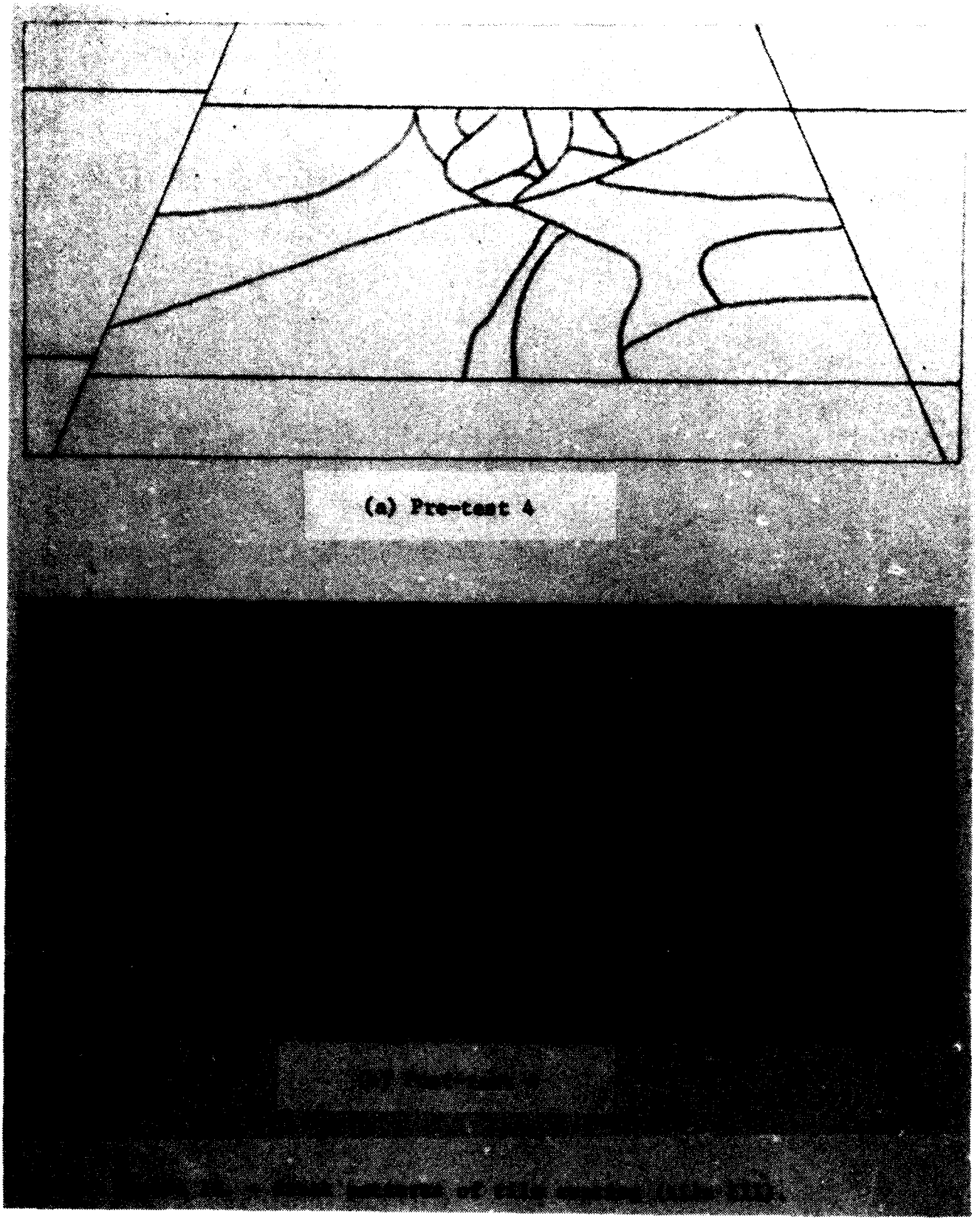

(a) Pre-test 4

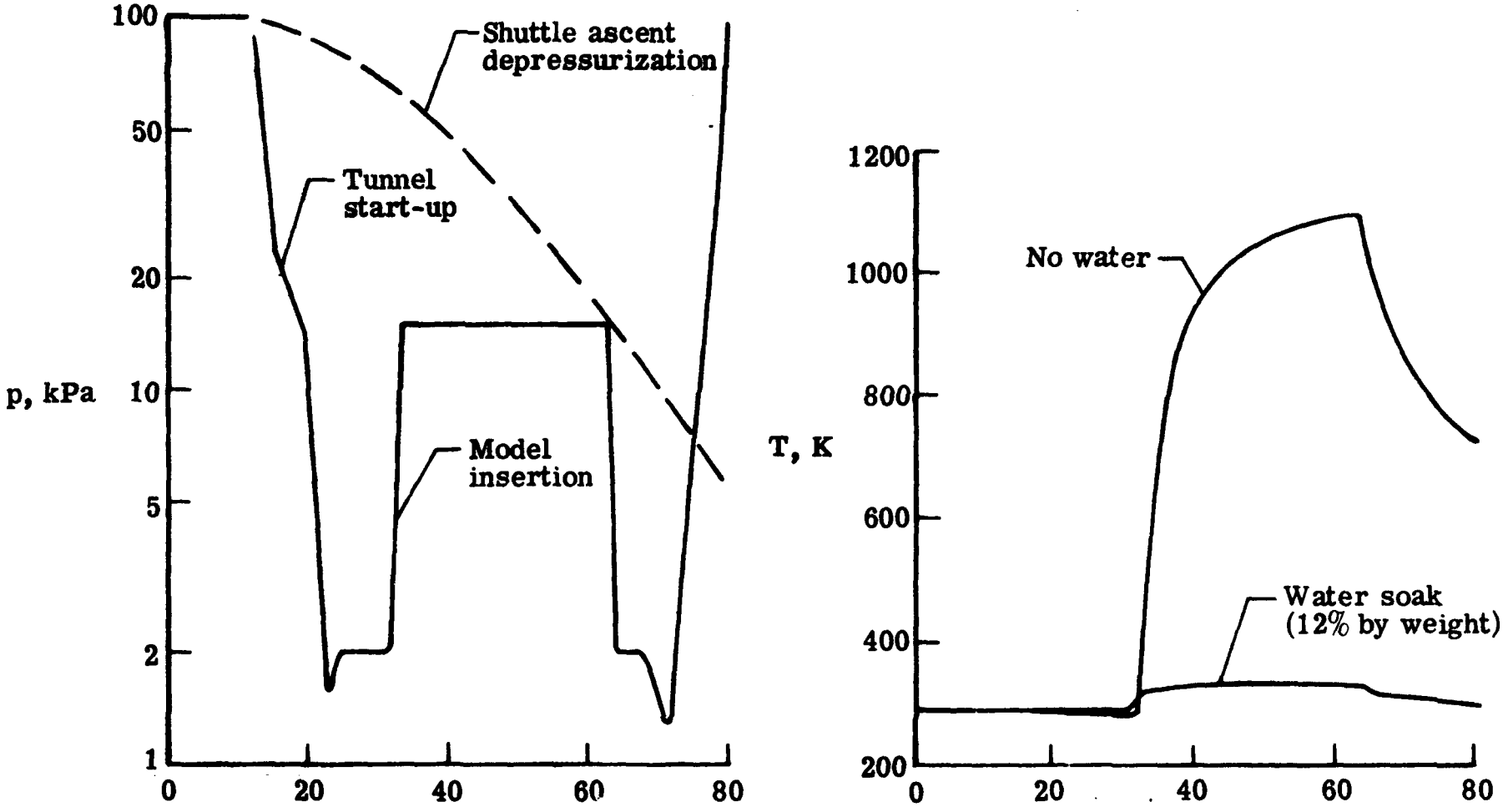

Figure 19.- Pressure-temperature history of LI-1542 tile with and without water soak.

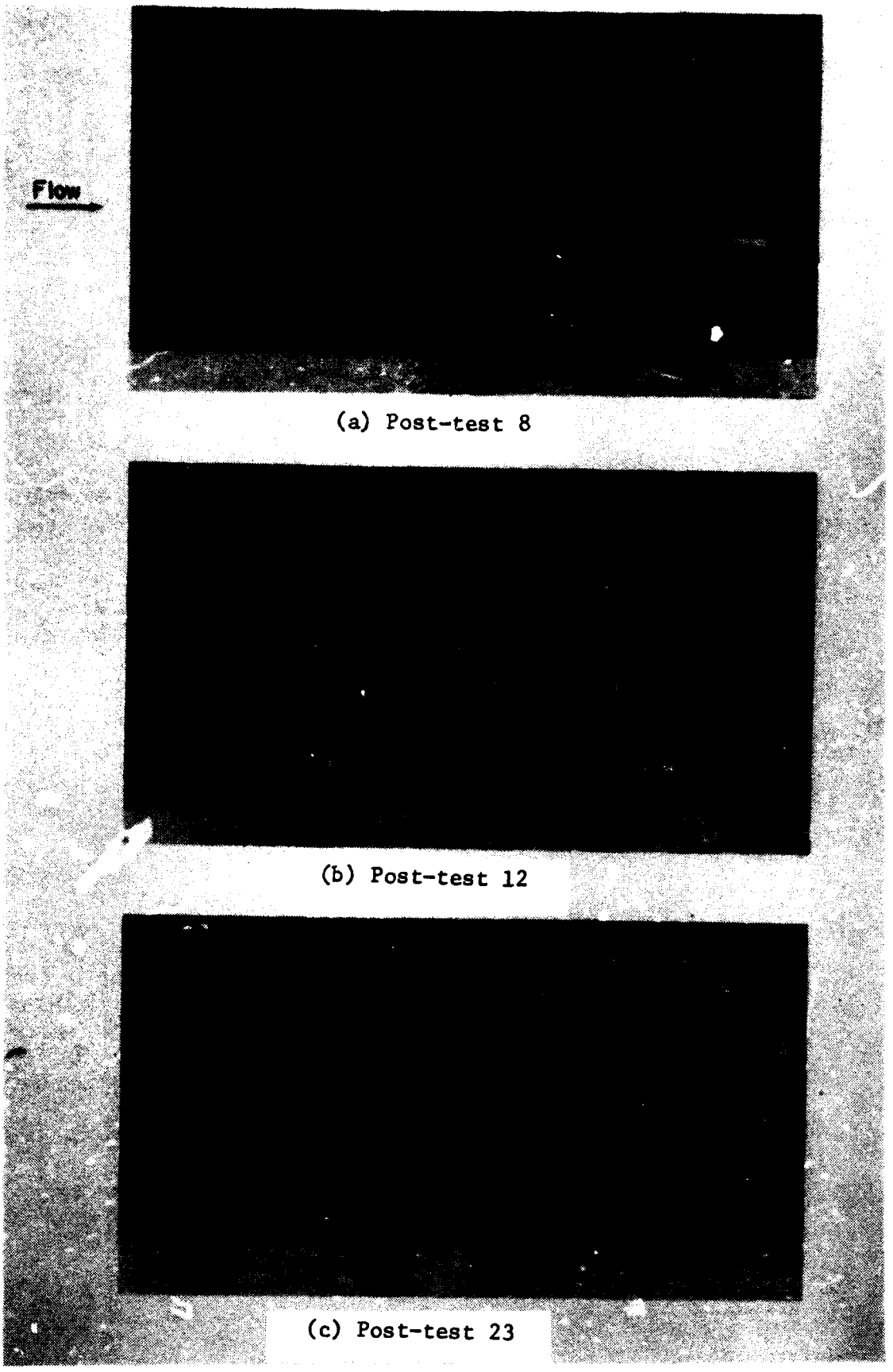

(a) Post-test 8

(b) Post-test 12

(c) Post-test 23

Figure 20. - History of crater damage and repair.

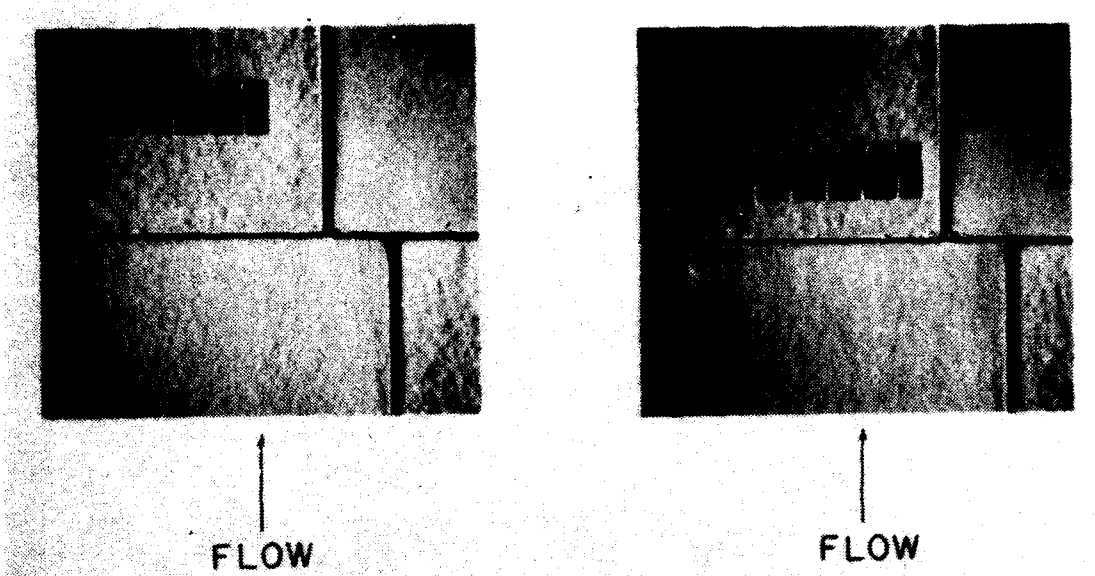

(a) Post test 2 (b) Post test 13

Figure 21. - Tile edge erosion of 0.6 mm forward-facing step at E3.

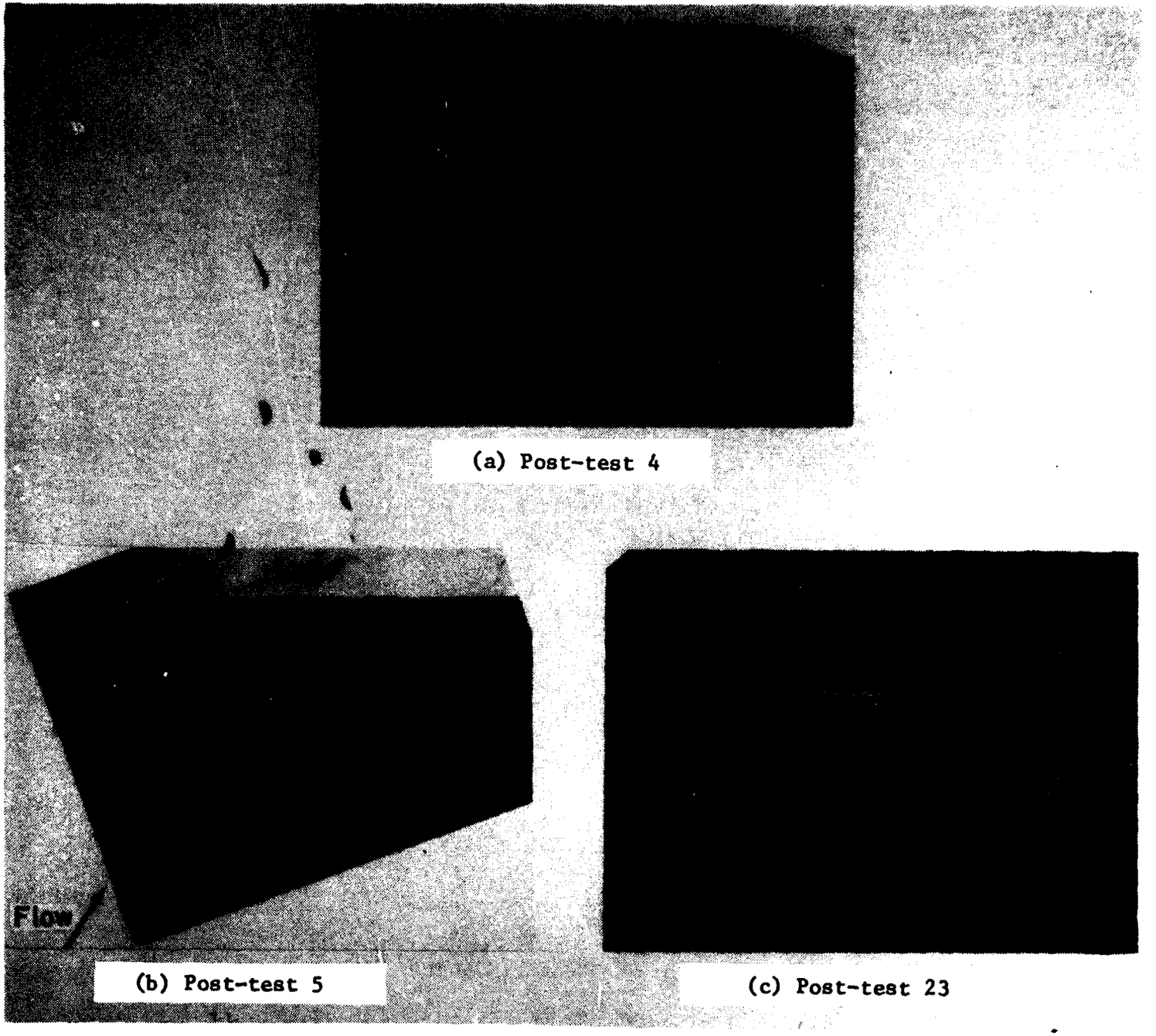

Figure 22. - Tile edge erosion of 0.4 mm forward-facing step along row I.

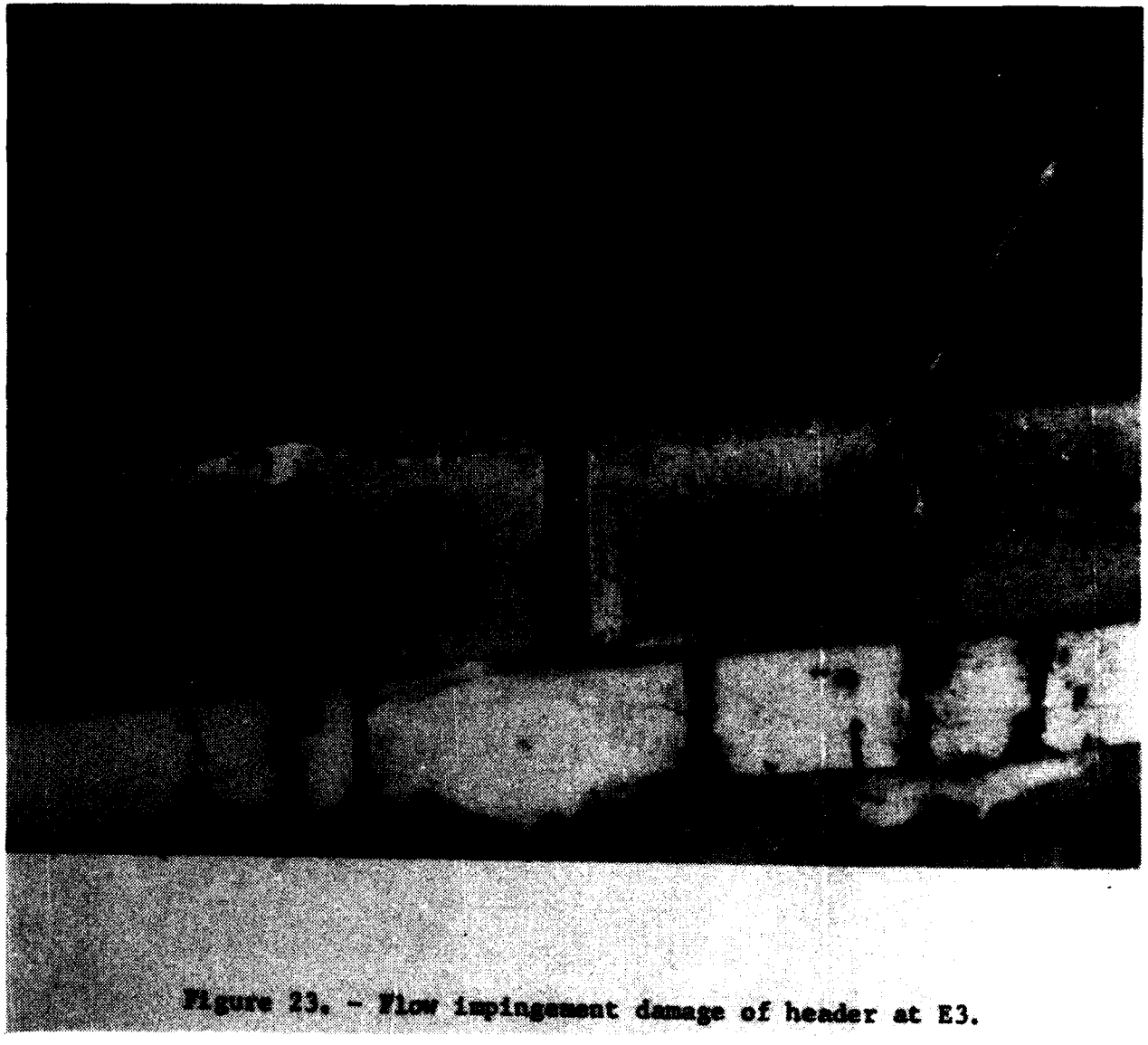

Figure 23. - Flow impingement damage of header at E3.